Earth's Future

RESEARCH ARTICLE
10.1029/2025EF006984

The Importance of Scale in the Future of Mangrove Blue Carbon Under Sea-Level Rise

A. P. Iwantoro[1,2], D. H. Urrego[1], D. Xie[3], A. P. Nicholas[1], K. A. Hapsari[4], J. A. Rodríguez-Rodríguez[5], J. C. Restrepo[6], J. Polanía[7], R. E. Aalto[1], L. F. Gómez Vargas[1], and B. van Maanen[1]

[1]Department of Geography, University of Exeter, Exeter, UK, [2]Coastal Processes Research Group, School of Biological and Marine Sciences, University of Plymouth, Plymouth, UK, [3]Department of Geographical Sciences, University of Maryland, College Park, MD, USA, [4]Department of Palynology and Climate Dynamics, University of Göttingen, Goettingen, Germany, [5]Centre for Nature Positive Solutions, RMIT University, Melbourne, VIC, Australia, [6]Departamento de Física y Geociencias, Universidad del Norte, Barranquilla, Colombia, [7]Departamento de Ciencias Forestales, Universidad Nacional de Colombia, Medellín, Colombia

Abstract As efficient carbon sinks, mangrove forests are crucial for climate change mitigation. However, their vulnerability to sea-level rise (SLR) and human activities influencing sediment supply introduces significant uncertainty regarding their future carbon storage capacity. Given the complexity of mangrove landscapes, current projections may be limited in their ability to capture the broad range of potential responses. Here we investigate the distinct drivers of local- and landscape-scale changes in mangrove carbon accumulation under SLR and changing fluvial sediment supply, by developing a novel eco-carbon-morphodynamic model. The model incorporates interactions between hydro-morphodynamic processes, mangrove dynamics, and carbon dynamics while tracking changes in bed composition accounting for organic and inorganic fractions. Numerical experiments are conducted using a schematized tidal embayment to systematically explore the impacts of different SLR rates and sediment supplies. Our results indicate that carbon accumulation can increase locally under SLR, in agreement with empirical data. However, at landscape-scale, SLR reduces total carbon accumulation by limiting areas for mangrove colonization. Also, mangrove mortality and erosion of carbon-rich soils cause a transition from a carbon sink to source. At intertidal scale, our findings indicate strong spatial variations in SLR rate thresholds for mangrove survival and carbon accumulation trajectories, linked to channel network dynamics. Local changes in carbon sequestration therefore do not necessarily reflect longer-term landscape-scale carbon stocks. Overall, our study highlights the scale-dependency of carbon accumulation responses and drivers, with internal system dynamics shown to be equally important as external forcings in determining mangrove vulnerability and carbon accumulation under future disturbances.

Plain Language Summary Mangrove forests effectively store carbon in the soil and are thus important in fighting climate change. However, their future carbon storage is uncertain due to rising sea levels and changes in sediment delivery from rivers, driven by climate change and human activities. To explore this, we created a new computational model linking coastal processes, mangrove growth, and carbon accumulation. We conducted our model simulations using a simplified tidal embayment, and tested scenarios with varying sea-level rise (SLR) and sediment supply. Results show that at specific locations within the mangrove forest, rising sea levels can increase carbon storage by promoting the production of carbon-rich organic material. However, across the entire coastal landscape, SLR generally reduces total carbon storage due to mangrove loss and soil erosion. This erosion can cause mangrove systems to shift from storing carbon to releasing carbon. We found strong local variations in how mangroves respond to SLR, influenced by changes in landscape patterns. Our findings emphasize that understanding the coastal landscape as a whole is crucial when predicting how mangroves might respond to climate and human-induced pressures, underscoring the need for new types of assessments and tools to better predict carbon dynamics and future climate change mitigation.

Key Points:

- sea-level rise (SLR) initially triggers enhanced carbon accumulation locally, but has a direct negative impact on landscape-scale carbon stocks
- Internal system dynamics can be equally important as external forcings in determining mangrove survival thresholds and carbon accumulation
- Mangrove mortality and erosion of carbon-rich soils due to SLR can ultimately cause a transition from a carbon sink to a source

Supporting Information:

Supporting Information may be found in the online version of this article.

Correspondence to:

A. P. Iwantoro,
arya.iwantoro@plymouth.ac.uk

Citation:

Iwantoro, A. P., Urrego, D. H., Xie, D., Nicholas, A. P., Hapsari, K. A., Rodríguez-Rodríguez, J. A., et al. (2026). The Importance of scale in the future of mangrove blue carbon under sea-level rise. *Earth's Future*, *14*, e2025EF006984. https://doi.org/10.1029/2025EF006984

Received 18 JUL 2025
Accepted 8 APR 2026

Author Contributions:

Conceptualization: A. P. Iwantoro, D. H. Urrego, A. P. Nicholas, B. van Maanen
Formal analysis: A. P. Iwantoro, K. A. Hapsari, J. A. Rodríguez-Rodríguez, B. van Maanen
Funding acquisition: D. H. Urrego, A. P. Nicholas, J. C. Restrepo, J. Polanía, R. E. Aalto, B. van Maanen
Investigation: A. P. Iwantoro, D. H. Urrego, K. A. Hapsari, B. van Maanen
Methodology: A. P. Iwantoro, D. H. Urrego, D. Xie, A. P. Nicholas, K. A. Hapsari, R. E. Aalto, B. van Maanen

1. Introduction

Mangrove forests are situated in coastal areas of tropical and subtropical regions, occupying intertidal areas in a wide range of geomorphological settings such as river deltas, estuaries, and embayments (Dürr et al., 2011; Rovai et al., 2018; Twilley et al., 2018; Worthington et al., 2020). These ecosystems provide numerous ecosystem

Project administration: D. H. Urrego, A. P. Nicholas, J. Polanía, B. van Maanen
Resources: D. H. Urrego, B. van Maanen
Software: A. P. Iwantoro, D. Xie
Supervision: D. H. Urrego, A. P. Nicholas, J. C. Restrepo, J. Polanía, R. E. Aalto, B. van Maanen
Validation: A. P. Iwantoro, K. A. Hapsari
Visualization: A. P. Iwantoro
Writing – original draft: A. P. Iwantoro, B. van Maanen
Writing – review & editing: A. P. Iwantoro, D. H. Urrego, D. Xie, A. P. Nicholas, K. A. Hapsari, J. A. Rodríguez-Rodríguez, J. C. Restrepo, J. Polanía, L. F. Gómez Vargas, B. van Maanen

services (Vo et al., 2012), including the capacity to store carbon. In fact, mangroves store a larger amount of carbon per area than terrestrial forests, often referred to as "blue carbon," with most of this carbon stored in the soil (Donato et al., 2011). Despite only covering less than 1% of the earth surface, they contribute around 15% of global ocean carbon storage (Alongi, 2012). The dynamics of carbon sequestration in mangrove environments are driven by various processes, including in situ preservation and decomposition of organic matter, such as dead roots and litter fall, as well as entrapment of sediment and associated carbon carried by tides and river flow (Kristensen et al., 2008). Over time, these processes lead to the accumulation of carbon, resulting in the formation of rich, carbon-dense soils. Therefore, in recent decades, carbon sequestered by mangroves has become a focus of interest because of its large potential for climate change mitigation (Alongi, 2014; Duarte et al., 2013). The efficiency of carbon accumulation processes in mangrove ecosystems is influenced by mangrove forest distributions and development within coastal systems., Mangrove dynamics, in turn, are driven by multiple drivers from local to global scale including, morphodynamic development, precipitation, temperature, CO_2 concentration, climatic events, sea level and human activities (Alongi, 2022; Cavanaugh et al., 2019; Lovelock & Reef, 2020; McKee et al., 2012; Rovai et al., 2018; Twilley et al., 2018; van Hespen et al., 2023; Worthington et al., 2020), such that the future of mangrove carbon sequestration is highly uncertain.

Sea-level change, especially, has been very prominent in shaping mangrove ecosystems and their carbon accumulation and storage function, by influencing the dynamics of coastal landforms that can promote the development of, drown or displace mangrove ecosystems (Alongi, 2012; Macreadie et al., 2019; Saintilan et al., 2020; Woodroffe et al., 2016). Sea-level rise (hereafter SLR) has drowned mangroves in the past and is projected to result in similar trend in the future in some area (Osland et al., 2024; Saintilan et al., 2020; Woodroffe et al., 2016). At the same time, mangroves have shown ability to withstand rising sea levels through complex bio-physical feedbacks and observations have shown that accretion rates in some mangrove ecosystems have so far kept pace with SLR (Alongi, 2021; Saintilan et al., 2020; Woodroffe et al., 2016). This is partly because increased inundation following SLR can enhance the trapping and deposition of mineral sediment (Krauss et al., 2010, 2014; Lovelock et al., 2010; McKee, 2011). Also, the accumulation of organic material may accelerate during SLR, such that carbon stocks may actually increase (Kelleway et al., 2016; Krauss et al., 2017; Lamont et al., 2020). Based on different SLR trajectories across different global regions, Rogers et al. (2019) therefore found that wetland ecosystems that experienced rapid SLR have higher carbon accumulation and storage compared to those wetlands with lower SLR rates. This is attributed to the fact that SLR creates additional accommodation space which is the space available for mineral and organic sediment accumulation (Jervey, 1988; Rogers, 2021). Still, despite these feedbacks enhancing mangrove resilience, there are limits to mangrove survival from SLR and Saintilan et al. (2020) identified a critical SLR rate threshold of around 7 mm yr^{-1} beyond which mangrove accretion may fail to keep pace. As SLR rates are projected to exceed this threshold, particularly in the high-emission scenario (RCP8.5), this may have drastic impacts on and increasing the uncertainty of mangroves ecosystems and related carbon accumulation in the future.

The accumulation of sediment that is needed for mangrove survival depends largely on sediment availability and thus the sediment supply to coastal areas (Lovelock et al., 2015). Mangroves in estuaries and embayments where sediment supply from rivers is abundant, and accretion processes enhance mangrove resilience to SLR, are therefore less vulnerable (Sasmito et al., 2016). However, increasing anthropogenic activities in river catchments such as river damming have led to sediment starvation in the coastal areas (Day et al., 2007; Ellis et al., 2004; Syvitski et al., 2009), thereby jeopardizing the opportunity for mangroves to counteract SLR. Conversely, upstream land conversion and deforestation increase allochthonous sediment supply, but the consequences for mangrove ecosystems are complex. First, while enhanced fluvial sediment supply to coastal areas promotes coastal accretion and has helped mangrove ecosystems to keep pace with SLR (Lovelock et al., 2015), it may be still insufficient for mangrove ecosystems to offset the increasing rates of SLR in the future. Second, excess sediment supply can also be detrimental, as it reduces the inundation period due to increasing accretion rates, degrades water quality and smothers mangrove roots, potentially threatening mangrove ecosystems (Ellison, 1999; Lugo & Snedaker, 1974; Nardin et al., 2021). As such, the impacts of changing sediment supply on mangrove forest development and vulnerability are still uncertain, particularly as SLR accelerates in the future.

While existing studies have indicated the importance of external forcing conditions (i.e., SLR rates and sediment supply) and the understanding of global and regional variability in mangrove resilience and carbon accumulation has advanced, we still have limited knowledge of intra-system variations in mangrove carbon dynamics and how these relate to landscape-scale responses. Here we use "landscape" to refer to the coastal eco-morphodynamic

landscape where channel networks, intertidal areas and mangrove vegetation are tightly connected system components. Advancing our understanding of landscape dynamics is particularly important because empirical data on sediment accumulation and subsurface processes are often sparse with typically limited coverage across a mangrove forest (Woodroffe et al., 2016), such that any intra-system variations can potentially hinder the extrapolation to larger scales. Intra-system variations are likely to exist, as mangrove responses are complex given the complexity of the morphodynamic behavior of the sedimentary systems that host these ecosystems (Woodroffe et al., 2016). Vertical bed elevation changes rely on numerous biophysical feedbacks, involving the deposition and erosion of organic and mineral sediment as well as the production and decomposition of organic matter (Alongi, 2011; McKee et al., 2020). Apart from vertical movements, mangroves can expand or erode laterally in response to morphological change and may retreat landwards in response to SLR (Kirwan & Megonigal, 2013). Morphological change in mangrove landscapes is typically linked to tidal channel network, which are known to control the spatial distribution of sediment accretion (Schwarz et al., 2022; Xie et al., 2023). Consequently, there will be significant spatial variability in morphological development within the system, leading to corresponding variability in mangrove vulnerability and carbon stock dynamics. At the same time, SLR may trigger changes in channel networks, including channel widening and deepening, channel migration and potential headward erosion (D'Alpaos et al., 2007; Van Maanen et al., 2015), with unknown effects on carbon dynamics. As a result, unraveling mangrove carbon dynamics and responses to SLR is extremely complex with different drivers operating at different spatial scales.

A numerical modeling approach can help to comprehensively evaluate mangrove carbon accumulation over various spatial and temporal scales. Numerical models have proven to be useful to extend our understanding of how natural systems respond to SLR and human-induced disturbances with detailed descriptions of the governing processes (e.g., Dissanayake et al., 2012; Sandi et al., 2021; Xie et al., 2023; Zhou et al., 2016). One notable limitation of existing models for mangrove ecosystems is that either the below-ground processes or above-ground processes are highly simplified. While some modeling studies have successfully coupled hydro-morphodynamics and mangrove growth (Beselly et al., 2023; Van Maanen et al., 2015; Wei et al., 2024; Xie et al., 2023), they neglected the complex processes controlling the accretion of carbon-rich organic matter. On the other hand, models that tend to focus on mangrove carbon dynamics are typically ran in isolation from above-ground processes, or lack detailed descriptions of sediment transport processes and coastal morphological change (Buffington et al., 2024; Chen & Twilley, 1999; Kirwan et al., 2010; Mack et al., 2023; Sandi et al., 2021; Schuerch et al., 2018; Wang et al., 2021). Clearly, there is a need to develop new models that include a more comprehensive treatment of both above-ground and below-ground processes to improve the predictions of future changes in mangrove forest distribution, morphodynamic development and carbon accumulation processes.

To fill these critical gaps, we here develop an eco-carbon-morphodynamic model to investigate the distinct drivers of both local-scale and landscape-scale changes in mangrove carbon accumulation under SLR and changing fluvial sediment supply. The new process-based model accounts for mangrove dynamics in both vertical and lateral dimensions, and incorporates mutual feedback among hydro-morphodynamic processes, vegetation dynamics, and carbon dynamics in biomass and soil. As a result, it allows us to unravel landscape-scale responses and intra-system variations of carbon dynamics under changing boundary conditions. The findings of this study provide critical insights into the importance of accounting for both spatial and temporal variability in morphodynamical processes and mangrove forest dynamics when managing blue carbon stocks in coastal wetlands under environmental changes.

2. Methodology

We developed and employed an eco-carbon-morphodynamic model that facilitates mutual interactions between the physical processes governing hydrodynamics and sediment transport (hydro-morphodynamics), the biological processes involved in mangrove forest development, and the carbon dynamics in mangrove ecosystems. This model involves three coupled models, namely (a) an open-source hydro-morphodynamic model, Delft3D v4.01.00 (Lesser et al., 2004) to simulate the physical conditions including hydrodynamic processes, sediment transport and morphological change within the system, (b) a dynamic vegetation model that builds upon previous work by Van Maanen et al. (2015) and Xie et al. (2020, 2023), and (c) a carbon dynamic model adapted from a well-established carbon model by Chen and Twilley (1999) (Figure 1).

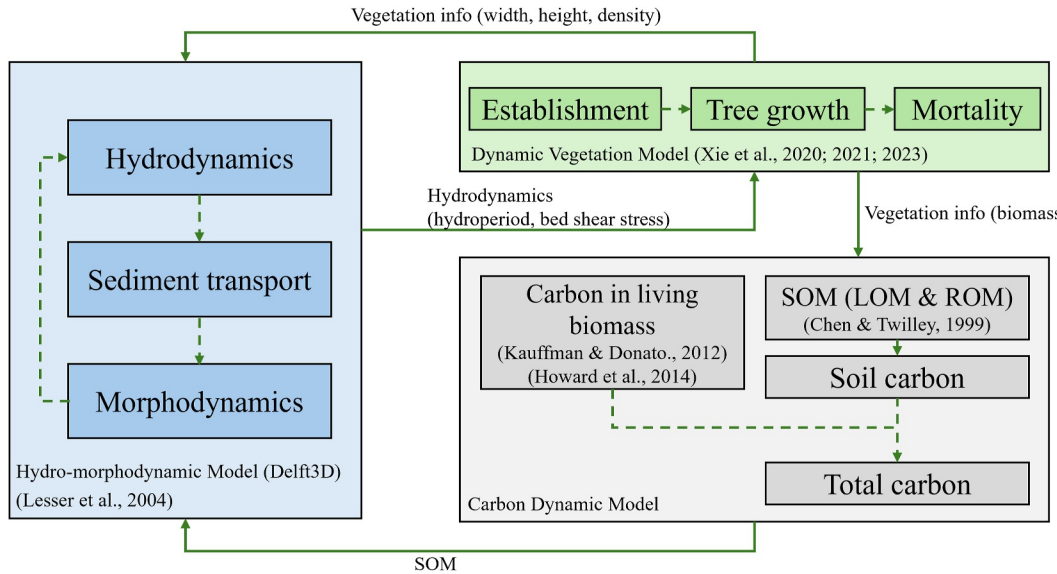

Figure 1. Eco-carbon-morphodynamic model framework, including the workflow inside each model and mutual feedback between models.

Delft3D computes the inundation regime and bed shear stress at each grid cell in the model domain. These parameters are required by the vegetation model to determine the suitability for mangrove colonization and evaluate subsequent growth and potential mortality. Meanwhile, the carbon model calculates (a) carbon in the living biomass and (b) most importantly, carbon in the soil through soil organic matter (hereafter SOM) production and decomposition based on the density and dimensions of the trees provided by the vegetation model and the existing amount of SOM. In turn, Delft3D receives information on the mangrove density and dimensions from the vegetation model so that the effects of mangroves on tidal currents can be incorporated, and bed elevation changes within the system are then determined by two main processes: (a) net sediment fluxes at the surface and (b) net belowground accumulation of SOM, as simulated by the carbon model. By implementing these feedback loops, this eco-carbon-morphodynamic model not only considers the changes in mangrove forest characteristics and its SOM accumulation but also accounts for organic matter erosion and transport driven by hydrodynamic forces and related morphological change. As a result, this approach provides a more comprehensive representation of carbon sequestration processes emerging from interactions within the coastal ecosystem.

In this paper, we provide a detailed description of the calculation methods and coupling approach of the carbon model (Figure 1). Parameter settings within the carbon dynamic model are provided within Section 2.1.3 where model equations are introduced, for ease of the reader. The Delft3D hydro-morphodynamic and mangrove vegetation models and their coupling are thoroughly described in Xie et al. (2020, 2022). Specific parameter settings for the hydro-morphodynamic and mangrove model are therefore provided in Section 2.2 where the model set-up is described. All parameter values are summarized in the Supporting Information S1.

2.1. Model Description

2.1.1. Hydro-Morphodynamic Model

The two-dimensional depth-averaged (2DH) version of Delft3D is employed to simulate the physical conditions within the system. Delft3D applies a semi-implicit numerical scheme on a staggered grid to solve the unsteady shallow water, sediment dynamic, morphological change equations (Lesser et al., 2004). This approach provides a detailed description of the hydrodynamic processes, including flow velocity and water level variations over the model domain. The derived hydrodynamic information is then used to compute sediment transport and resulting morphological changes within the system. Transport fluxes of sand are computed with the Engelund and Hansen (1967) formula, while horizontal transport of mud is governed by the advection-diffusion equation. Mud fluxes between the water column and the bed, that induce erosion and accretion processes, are calculated with the well-known Partheniades-Krone formulations (Partheniades, 1965). The same parameterizations and calculations

used for mud were applied to SOM to simulate its fluxes between the bed and the water, as suggested by Black et al. (2002), and thus the model represents SOM transport only within the water column without simulating atmosphere–ocean carbon fluxes. Notably, Delft3D allows for the simulations of multiple sediment compositions and vertical stratification within soil layers. Therefore, it is suitable for simulating fluvial, estuarine, and muddy coastal environments where mixed sediments and their vertical distribution are prevalent (e.g., Braat et al., 2017; Xie et al., 2023; Zhou et al., 2015). A detailed description of the Delft3D model can be found in Lesser et al. (2004).

The capability of Delft3D as a tool to investigate vegetated coastlines has been demonstrated in numerous studies (e.g., Brückner et al., 2019; van Oorschot et al., 2016; Xie et al., 2022, 2023; Zhou et al., 2015, 2016). While the Chézy formulation accounts for bed friction-induced flow resistance, an additional term is implemented to represent the flow resistance induced by vegetation. This additional resistance term is based on the approach proposed by Baptist et al. (2007) that allows two-way interaction between physical and biological processes.

2.1.2. Dynamic Vegetation Model

The dynamic vegetation model applies Matlab R2022b to simulate the behaviors of mangrove forests based on the physical conditions from Delft3D. The coupling mechanisms between Delft3D and this model are based on the framework proposed by Xie et al. (2020, 2022) that implements the approach by Van Maanen et al. (2015). Consistent with this framework, mangrove establishment and growth are controlled by the local hydrodynamic regime (from Delft3D outputs) and competition among neighboring vegetation, and the model does not explicitly represent atmospheric forcing (e.g., CO_2 concentration or temperature trends).

In the model, the establishment of mangrove seedlings was assumed to be dependent on two physical conditions: (a) appropriate inundation regime and (b) limited hydrodynamic forces. To evaluate whether the inundation regime is appropriate for mangrove seedlings, the model utilizes the analysis of relative hydroperiod (HP). HP is calculated as the proportion of time that a specific grid cell is inundated. Beyond the inundation requirement, limited hydrodynamic force is also required, often referred to as "windows of opportunity" (Balke et al., 2011; Friess et al., 2012) and is implemented by adopting a critical bed shear stress threshold for successful seedling establishment.

After mangrove colonization, the growth of mangrove trees is parameterized by increases in stem diameter, and height. Stem diameter then determines the number of root elements of a tree (Van Maanen et al., 2015). Growth rates are assumed to be related to local flooding and available resources (Berger & Hildenbrandt, 2000; Chen & Twilley, 1999; Van Maanen et al., 2015). The effect of local flooding on mangrove growth is quantified as a function of HP. A fitness function based on HP is implemented using the following expression:

$$f = \mathrm{HP}^2 \cdot a + \mathrm{HP} \cdot b + c \tag{1}$$

where the constants a, b and c are calibrated to represent optimal mangrove growth, and the values used were −2, 1.5, and 0.75, respectively. Equation 1 implies that optimal growth conditions (i.e., f (HP) = 1) are reached when HP = 0.25. Growth quality declines as the relative hydroperiod deviates from this optimal value.

Furthermore, limited resource availability is expressed by the competition stress factor (C), which reflects competition between individual trees and surrounding vegetation. This factor is linked to the mangrove biomass (B) in a grid cell (Van Maanen et al., 2015):

$$C = \frac{1}{1 + \exp[\mathrm{d}(B_{\mathrm{crit}} - B)]} \tag{2}$$

where d is a constant controlling the rate of decline in C with increasing biomass and set to a value of −0.00005 as suggested by Van Maanen et al. (2015). B_{crit} represents the biomass when $C = 0.5$ and indicates when competition may lead to tree mortality. Mortality of mangrove trees occurs under reduced growth conditions and is implemented by evaluating the value of C. When $C < 0.5$ for 5 consecutive years, trees are removed to reduce local competition until growth conditions have improved sufficiently. A detailed description and parameterization of the dynamic vegetation model is provided in Xie et al. (2020, 2022).

2.1.3. Carbon Dynamic Model

The carbon dynamic model simulates carbon stocks by considering both living biomass and the vertical distribution of carbon in the soil through SOM. The model calculates carbon from living biomass by converting the aboveground and belowground biomass provided by the vegetation model. Meanwhile, soil carbon stocks receive inputs from leaf and twig litter accumulating in the topsoil layer, as well as dead root turnover throughout the soil profile.

Conversion factors are used to estimate the carbon content of the living biomass. Aboveground biomass is converted into carbon using the following expression

$$C_{\mathrm{ag}} = F_1 \cdot B \tag{3}$$

where F_1 is a constant factor of 0.47 as recommended by Kauffman and Donato (2012) and Howard et al. (2014). Meanwhile, carbon content from belowground living biomass is calculated as follows

$$C_{\mathrm{bg}} = F_2 \cdot F_3 \cdot B. \tag{4}$$

For mangroves, the value of F_2 is variable, as observations suggest that F_2 increases with higher soil salinity (Saintilan, 1997). Sandi et al. (2021) applied a range of values (0.5–2) that exponentially rise with decreasing HP. As we assume uniform salinity, we adopted a constant F_2 value of 1 as implemented by other studies (e.g., Lamont et al., 2020; Meng et al., 2021). F_3 is a constant for root biomass conversion. We applied the value of 0.39 as recommended by Howard et al. (2014) and Jaramillo et al. (2003).

For soil carbon, SOM is partitioned into two pools based on decomposition rates: labile organic matter (LOM), which has a rapid decomposition rate and refractory organic matter (ROM), which has a slower decomposition rate (Chen & Twilley, 1999). Both LOM and ROM are calculated for each vertical layer within the soil profile. Furthermore, SOM is converted to carbon as follows

$$C_{\mathrm{soil}} = F_4 \cdot (\mathrm{LOM} + \mathrm{ROM}) \tag{5}$$

where F_4 is a constant of SOM conversion. Given our use of a schematized tidal embayment setting in this study (as described in Section 2.2), we adopted the average F_4 value (0.472) observed by Breithaupt et al. (2023) for embayments with terrigenous settings.

In the topsoil layer, the model calculates LOM and ROM by incorporating leaf and twig litter in addition to dead root turnover, building on the work from Chen and Twilley (1999) as follows

$$\begin{aligned}\mathrm{LOM}(t+1) = {} & [\mathrm{LOM}(t) - k_b \cdot \mathrm{LOM}(t)] + [\mathrm{LOM}_{\mathrm{LT}}(t+1) - k_a \cdot \mathrm{LOM}_{\mathrm{LT}}(t+1)] + \big[(1 \\ & - f_{c1}) \cdot \mathrm{FRP}(t+1) + (1 - f_{c2}) \cdot \mathrm{LRP}(t+1)\big] \cdot (1 - c_1) + \mathrm{ROM}(t) \cdot k_c (1 - f_2),\end{aligned} \tag{6}$$

$$\begin{aligned}\mathrm{ROM}(t+1) = {} & \{[\mathrm{ROM}(t) + \mathrm{ROM}_{\mathrm{LT}}(t+1)] - k_c \cdot [\mathrm{ROM}(t) + \mathrm{ROM}_{\mathrm{LT}}(t+1)]\} + \big[f_{c1} \cdot \mathrm{FRP}(t+1) \\ & + f_{c2} \cdot \mathrm{LRP}(t+1)\big] \cdot (1 - c_1) + k_b \cdot \mathrm{LOM}(t) \cdot f_3\end{aligned} \tag{7}$$

In the other high-resolution soil layers below the topsoil, LOM and ROM are calculated based only on dead root turnover, as follows:

$$\begin{aligned}\mathrm{LOM}(t+1) = {} & [\mathrm{LOM}(t) - k_b \cdot \mathrm{LOM}(t)] + \big[(1 - f_{c1}) \cdot \mathrm{FRP}(t+1) + (1 - f_{c2}) \cdot \mathrm{LRP}(t+1)\big] \cdot (1 - c_1) \\ & + \mathrm{ROM}(t) \cdot k_c (1 - f_2),\end{aligned} \tag{8}$$

$$\begin{aligned}\mathrm{ROM}(t+1) = {} & [\mathrm{ROM}(t) - k_c \cdot \mathrm{ROM}(t)] + \big[f_{c1} \cdot \mathrm{FRP}(t+1) + f_{c2} \cdot \mathrm{LRP}(t+1)\big] \cdot (1 - c_1) \\ & + k_b \cdot \mathrm{LOM}(t) \cdot f_3.\end{aligned} \tag{9}$$

t indicates time within the simulation. Thus, LOM(t) and ROM(t) represent the SOM already present in the soil at the initial condition or at the previous time step while LOM(t+1) and ROM(t+1) are the SOM at the current timestep within the simulation. f_{c1} and f_{c2} are the portions of fine and large roots entering ROM with a value of 0.25 and 0.2, respectively (Chen & Twilley, 1999). The model incorporates decay constants for different SOM pools: k_a for LOM from litter (0.9 years^{-1}), k_b for existing LOM in the soil (0.256 years^{-1}), and k_c for ROM (0.001 years^{-1}) (Chen & Twilley, 1999). c_1 (0.1) is the ash content of litter (Benner et al., 1990). f_2 (0.45) represents the mass loss because of respiration for both dead wood and twig litter (Parton et al., 1987). f_3 is the fraction of decomposing LOM that transitions into ROM and set to 0.004 (Chen & Twilley, 1999). $\mathrm{LOM_{LT}}$ and $\mathrm{ROM_{LT}}$ are the contribution of leaf and twig litter in the topsoil layer expressed by

$$\mathrm{LOM_{LT}} = \mathrm{NLP} \cdot (1 - c_0) \cdot (1 - c_1) \tag{10}$$

$$\mathrm{ROM_{LT}} = \left[c_0 \cdot \mathrm{NLP} + \left(1 - f_2\right) \cdot k_t \cdot \mathrm{NTP}\right](1 - c_1) \tag{11}$$

where c_0 (0.15) is the portion of lignin content in leaf litter that becomes ROM, while the remaining fraction contributes to LOM (Benner et al., 1990). k_t (0.276 years^{-1}) is the specific decay constant for twigs (Robertson & Daniel, 1989). According to Chen and Twilley (1999), NLP and NTP are the net accumulation of leaf and twig litter, respectively. They are estimated by

$$\mathrm{NLP} = f_1 \cdot \mathrm{LP} \cdot (1 - k_e) \tag{12}$$

$$\mathrm{NTP} = \left(1 - f_1\right) \cdot \mathrm{LP} \cdot \ (1 - k_e). \tag{13}$$

In these equations, f_1 is a ratio of leaf litter to total litter with a value of 0.7 (Pool et al., 1975; Twilley et al., 1986). The remaining litter fraction is assumed to be twigs. k_e is the rate of litter export set to 0.4 years^{-1} (Chen & Twilley, 1999), accounting for losses due to hydrology, topography, and human activities (Twilley et al., 1997). Finally, LP is the rate of litter production that is directly related to the forest basal area (Chen & Twilley, 1999) as follows

$$\mathrm{LP} = 1.33 + 0.292\ \mathrm{BA}. \tag{14}$$

Furthermore, the model estimates the turnover rate of dead roots by calculating the fine root production and large root production entering the soil (FRP and LRP in Equations 6–9), following the approach of Chen and Twilley (1999). FRP and LRP are expressed as

$$\mathrm{FRP}(z) = k_r \cdot R(z) \tag{15}$$

$$\mathrm{LRP}(z) = k_m \cdot R(z). \tag{16}$$

In these equations, k_r represents the turnover rate of fine roots (0.5 years^{-1}) (Chen & Twilley, 1999), and k_m represents the turnover rate of main roots (0.1 yr^{-1}), estimated using the decay rate of wood (Chen & Twilley, 1999). R is the vertical distribution of mangrove root biomass. It is described by an exponential function of soil depth proposed by Komiyama (1989).

$$R(z) = R(0)\, e^{-e_{\mathrm{RP}} z} \tag{17}$$

where $R(0)$ represents the root mass at the top soil layer, z is the soil depth, and e_{RP} is the attenuation rate with a value of 0.04 cm^{-1} (Komiyama, 1989).

SOM may also accumulate in deep soil layers where roots are not present and areas beyond the mangrove forests. The presence of SOM in these locations can be attributed to three main processes: (a) sedimentation processes that bury SOM originally produced in the upper layers, (b) erosion and transport of SOM from mangrove forests driven by hydrodynamic forcings that lead to its accumulation beyond the forest boundaries, and (c) SOM originating from former mangrove trees that are no longer present. Here, LOM and ROM decompose following:

$$\mathrm{LOM}(t+1) = [\mathrm{LOM}(t) - k_b \cdot \mathrm{LOM}(t)], \quad (18)$$

$$\mathrm{ROM}(t+1) = [\mathrm{ROM}(t) - k_c \cdot \mathrm{ROM}(t)]. \quad (19)$$

Finally, after calculating LOM and ROM, their updated masses are used to update the bed level and sediment composition in the seabed for the next time step of the Delft3D simulation. In Delft3D, when hydrodynamic forces lead to soil erosion, both LOM and ROM are also eroded and transported accordingly.

2.2. Model Setup

Our approach uses idealized numerical simulations to unravel the controlling processes and eco-carbon-morphodynamic interactions driving changes in carbon stocks under SLR at different spatial scales. We intentionally simplify boundary and initial conditions to facilitate model interpretations (Murray, 2007). Although we do not simulate specific sites, we design our simulations based on existing literature describing mangrove growth conditions, such that our model insights are broadly applicable. As our new eco-carbon-morphodynamic model is based on three pre-existing models that were developed separately, parameter settings are based on previous studies with adopted values stemming from a range of different empirical data and modeling sources. This again hinders a direct comparison with specific field sites and model performance is therefore evaluated instead by comparing model behaviors and trends (Murray, 2013) and ensuring that key simulated variables, such as accumulation rates of organic matter and carbon, fall within the range of values typically observed in nature.

As many mangrove systems are situated within sheltered tidal environments (Woodroffe et al., 2016), we developed a schematized tidal embayment for our model simulations (Figure 2). The embayment has a length of 10 km and a width of 5 km, to represent typical mangrove environments and allow for a comparison with previous modeling studies (Boechat Albernaz et al., 2023; Marciano et al., 2005; Van Maanen et al., 2015; Xie et al., 2023; Zhou et al., 2014). The initial bathymetry within the embayment was set to a uniform depth of 2 m. An offshore part extends 5 km from the inlet and stretches 10 km along the open coast. It gradually deepens from the inlet toward the offshore boundary, reaching a maximum depth of 25 m. This spatial domain was discretized by 50 × 50 m grid cells and Delft3D simulations were run with a time step of 0.25 min to ensure the numerical stability.

Two types of open boundaries were defined, namely offshore and upstream river boundaries. The offshore boundaries are located at the east, south and north end of the offshore part in the model domain. A semi-diurnal tidal component (S_2) with an amplitude of 1 m was imposed on the eastern boundary. Meanwhile, the north and south boundary applied a Neumann boundary condition (null gradient) as applied in previous modeling studies on vegetated embayments (e.g., Xie et al., 2023; Zhou et al., 2016). The influences of other oceanic forces, including wind, waves, Coriolis force, density differences, were considered minimal and therefore neglected. Two river boundaries were defined in the model to represent river inflow to the embayment, one at the western edge of the embayment and one at the southern edge. Each boundary has a width of 300 m and a constant river discharge of 300 m^3s^{-1} such that reasonable width-depth ratios and flow velocities are ensured (Boechat Albernaz et al., 2020).

The initial sediment composition throughout the domain is uniform, consisting of fine sand defined by a median grain size (D_{50}) of 0.2 mm. During the simulation, additional sand input was imposed from the river and offshore boundaries that is in equilibrium with the flow conditions and respective sediment transport rates. Meanwhile, a suspended sediment concentration (SSC) of cohesive sediment (mud) with a settling velocity (w_s) of 0.2 mm s^{-1} was also imposed at the river boundaries. The critical bed shear stress for erosion (τ_{ce}) and deposition (τ_{cd}) of mud were set to 0.25 N m^{-2} and 1,000 N m^{-2}, respectively, as implemented by Xie et al. (2023). The high τ_{cd} was set since numerous studies have shown that deposition occurs continuously, suggesting that there is no specific threshold required for deposition (Sanford, 2008).

In the dynamic vegetation model, multiple species can be defined in the model (Xie et al., 2020). However, since we focus here on geomorphic-carbon linkages and how these processes respond to external disturbances, a monospecific forest composition was considered in the model. *Avicennia marina* was selected as a representative mangrove species following other mangrove modeling studies (Van Maanen et al., 2015; Xie et al., 2022, 2023). Xie et al. (2022) suggested that grid cells inundated less than half of the time (i.e., $0 < HP < 0.5$) are appropriate

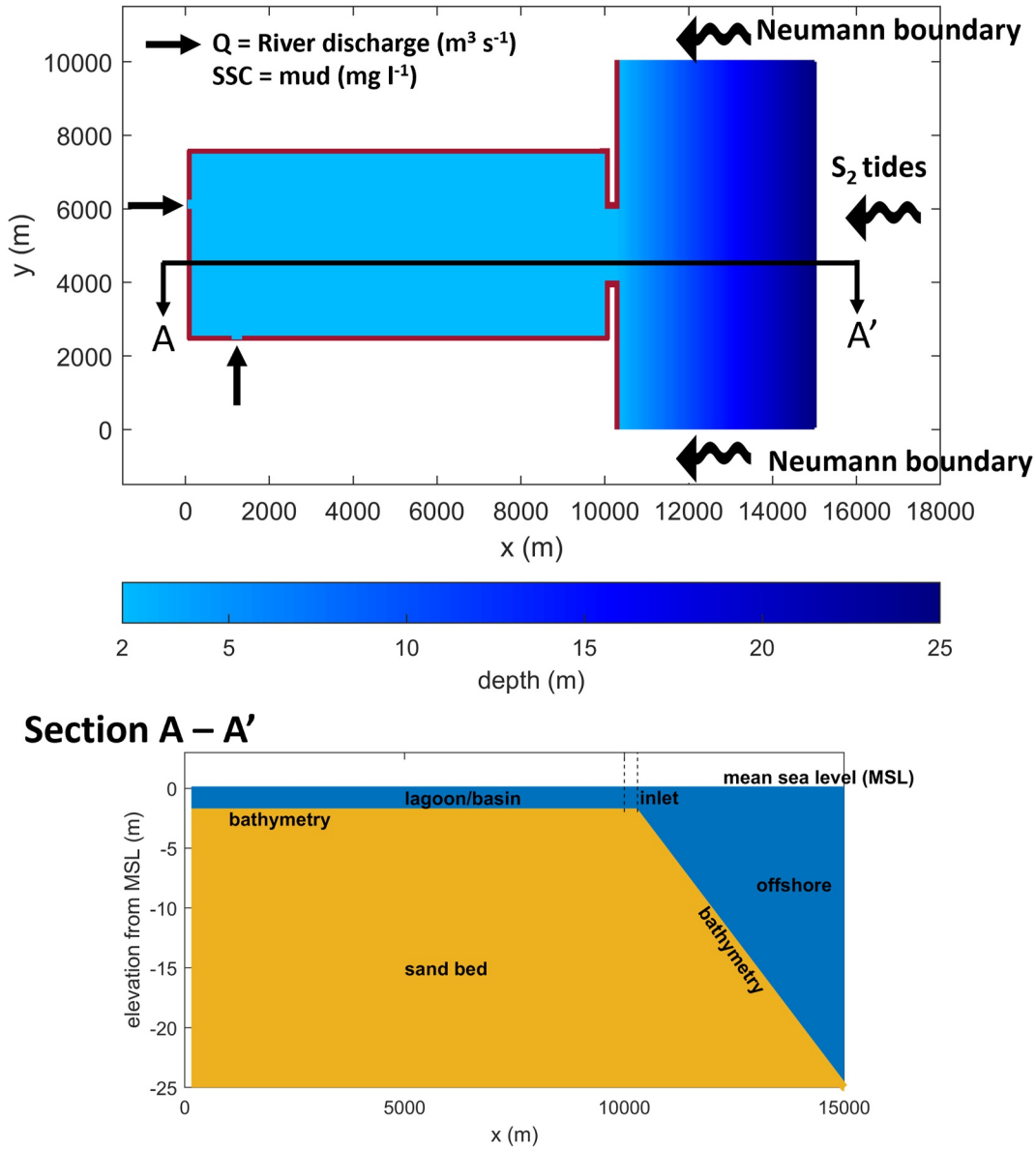

Figure 2. The schematized tidal embayment built in this study and its longitudinal transect across the embayment, including the boundary conditions at each open boundary and bathymetry.

for *Avicennia marina* colonization. For areas deemed suitable based on inundation, the 90th percentile bed shear stress was evaluated and 0.2 N/m^2 was set as a threshold for successful mangrove colonization as suggested by Balke et al. (2011). If the conditions for mangrove establishment are met, the model assigns an initial number of seedlings per unit area, considering the maximum density that a grid cell can support. In this case, we set the initial density to 3,000 seedlings per hectare, with an initial stem diameter of 1.37 cm (Berger & Hildenbrandt, 2000; Van Maanen et al., 2015).

To simulate the vertical distribution of SOM and therefore carbon burial, vertical stratification of the seabed soil was defined in Delft3D. The soil is stratified into 30 layers with high resolution (10 cm) and a thick bottom layer (47 m) to ensure sufficient sediment availability for erosion. Bed elevation change within the simulation is treated by a Lagrangian framework. In this framework, the thickness of the high-resolution layers remains constant, and these layers move with the erosion and accretion processes. The advantage of this framework is that it prevents thickness changes of the high-resolution layers while allowing individual sediment fractions to change in each layer based on morphodynamic processes, and SOM production and decomposition. The bottom layer, however,

changes during the simulation depending on the erosion, accretion and SOM production as well as decomposition processes at each grid cell. Its thickness decreases with erosion and SOM decomposition while increases with accretion and SOM production. As a result, the model can track the distribution of carbon due to morphodynamic processes simulated in Delft3D as well as SOM production and decomposition simulated in the carbon dynamic model across all cells with the desired resolution throughout the simulation. The schematization for the interaction between Delft3D, dynamic vegetation model and carbon dynamic model to simulate the vertical distribution of SOM dynamics within the soil is illustrated in Figure S1 in Supporting Information S1.

To expedite the morphodynamic calculations in Delft3D, the bed level change resulting from sediment transport and erosion-deposition processes was multiplied with a morphological acceleration factor (Morfac). The application of Morfac has been implemented in bio-morphodynamic modeling studies of tide-influence systems (e.g., Xie et al., 2023; Zhou et al., 2016). In this study, we applied a Morfac value of 90, indicating that a one-day hydrodynamic simulation period corresponds to three months of morphological change. The growth of mangroves and carbon dynamics follow this morphological timescale, with mangrove growth updated every 3 months and carbon production-decomposition processes updated annually.

Model evaluation was conducted by comparing C_{soil} sequestration rates and SOM accretion from the model results with available measurements from other studies (i.e., Alongi, 2014; McKee, 2011) provided in Figure S5 in Supporting Information S1. This comparison ensured that the model accurately captured key dynamics in mangrove carbon storage and SOM processes with suitable parameter settings.

2.3. Defined Cases

A spin-up simulation was first conducted before examining the effect of SLR and fluvial SSC changes on mangrove carbon dynamics. The spin-up simulation was run for 150 years such that morphological equilibrium at the inlet was achieved (similar to Xie et al., 2023) and a mature mangrove forest was established within the embayment. In this study, morphological equilibrium refers to an operationally defined quasi-stable inlet/entrance morphology (i.e., small decadal bed-level change), rather than a fully static system or steady biomass/soil-carbon stocks. Mangrove coverage and the spatial extent of carbon-rich soils may continue to increase over longer timescales as the embayment progressively infills and intertidal platform continues to expand under sustained sediment supply. The latter is indicated by a nearly constant biomass at grid cells where mature mangrove forest is present. Spin-up simulation results are provided in the Supporting Information S1. During the spin-up simulation, the mean sea level was kept constant, implying no sea-level change. Additionally, a constant SSC of 20 mg/l was imposed from each river. This value aligns with typical SSC levels observed in natural mangrove forests, as reported by Lovelock et al. (2015).

Following the spin-up, three cases were employed to explore how SLR and fluvial SSC changes influence mangrove carbon dynamics. The first case, the Default Case, serves as a baseline for comparison. It extends the spin-up simulation in the absence of SLR and a constant SSC of 20 mg/l. The second case, the SLR Case, investigates the effects of different SLR scenarios. Three simulations were run under this case, representing low, medium, and high SLR conditions using trajectories labeled RCP2.6, RCP4.5, and RCP8.5, respectively. Projections of SLR were implemented by incrementally raising the water level at the seaward boundary following three prescribed trajectories selected to span a wide range of end-century SLR conditions: the 5th percentile of RCP2.6 (0.29 m by 2,100), the median (50th percentile) of RCP4.5 (0.55 m by 2,100), and the 95th percentile of RCP8.5 (1.1 m by 2,100), all relative to 1986–2005 average, following IPCC (2013) and Pörtner et al. (2019). The scenario set was designed to bracket low, intermediate, and high SLR forcing conditions, rather than to compare the central trajectories of all three RCPs. These IPCC scenario labels (RCP2.6/4.5/8.5) are used only as shorthand for the prescribed SLR trajectories, not to imply that the full suite of RCP-associated atmospheric forcings is applied in the coupled model. The IPCC Sixth Assessment Report (AR6) subsequently updated and expanded the assessment of sea-level projections and uncertainty, and further highlighted low-likelihood, high-impact outcomes associated with Antarctic ice-sheet processes (Fox-Kemper et al., 2021). However, the prescribed trajectories adopted in this study remain sufficiently similar for the purposes of the present process-based modeling because they span a comparable range of end-century SLR conditions. For instance, relative to the 1995–2014 average, AR6 projected likely global mean SLR by 2,100 of 0.32–0.62 m under SSP1-2.6, 0.44–0.76 m with the central value of 0.56 under SSP2-4.5, and 0.63–1.01 m under SSP5-8.5 (Fox-Kemper et al., 2021). Details regarding the rising mean water level through time for each SLR scenario are provided in the Supporting

Table 1
Summary of Suspended Sediment Concentration and Sea-Level Rise Imposed for All Simulations in This Study

Case	SSC (mg l^{-1})	SLR
Default Case	20	–
SLR Case	20	RCP2.6 (low SLR)
		RCP4.5 (medium SLR)
		RCP8.5 (high SLR)
SSC Case	10 (low SSC)	RCP8.5 (high SLR)
	20 (default SSC)	
	30 (high SSC)	

Note. The imposed SLR trajectories were selected to span a wide range of SLR conditions, using the lower-end RCP2.6 trajectory, the central RCP4.5 trajectory, and the upper-end RCP8.5 trajectory, following IPCC (2013) and Pörtner et al. (2019). These were implemented as changes in modeled mean water level through time.

Information S1. The third case, the SSC Case, explores the impact of different fluvial SSC imposed at the upstream river boundaries. Three simulations were conducted with different SSC levels: (a) low (10 mg/l), (b) default (20 mg/l), and (c) high (30 mg/l). These values were chosen based on reported SSC ranges for mangrove forests (Lovelock et al., 2015). For this case, the high SLR scenario RCP8.5 was used to explore the impact of changing sediment supply in the case of more extreme SLR. The summary of all cases is provided in Table 1.

3. Results

3.1. Landscape-Scale Dynamics

Morphological development, with the formation of tidal channels and intertidal areas in particular, allows for the colonization of mangroves. At the end of the spin-up simulation (year 0), approximately 40% of the embayment is covered with mangroves (Figure 3a), resulting in carbon-rich soils in a large portion of the basin (Figure 4a). In the absence of SLR, ongoing sediment accumulation raises the bed level and expands intertidal areas, which in turn reduces tidal prism (Figure 5a) and accommodation space (Figure 5b), while enhancing mangrove forest coverage (Figures 3b, 3c and 5e), total biomass (Figure 5d) and total C_{soil} stock (Figures 4b, 4c and 5g). However, the increase of bed levels toward high water level leads to expansion of areas that experience increased stress because of limited hydroperiods. This results in suboptimal growth conditions and thereby lower biomass within the forests as indicated by transitions from dark to lighter green shading in Figures 3a–3c and decreasing biomass density in Figure 5f, contributing to a slight decline in total C_{soil} input rates (Figure 5h).

Strong temporal variability is also evident across all SLR scenarios (Figures 3d–3m, 4d–4m and 5d–5h). SLR increases accommodation space (Figure 5b), which triggers enhanced mud deposition within the basin (Figure 5c) allowing bed levels to increase. Still, despite increasing mangrove elevations, rising sea levels progressively diminish suitable areas for mangrove growth especially in the RCP8.5 scenario (Figure 5e). Interestingly, while mangrove area expansion slows or even declines almost immediately following the onset of SLR (Figure 5e), total mangrove biomass initially maintains levels comparable to the default scenario (Figure 5d). The duration of this phase, during which biomass continues to increase despite rising sea levels, depends on the forcing conditions. While total mangrove biomass continues to increase under RCP2.6, biomass eventually decreases in all other scenarios with the onset of this decline happening earlier under higher SLR scenarios and lower sediment supply (Figure 5d). In any case, the initial continuation of increasing total biomass (Figure 5d) and immediate decline in forest area (Figure 5e) is linked to higher biomass densities in the remaining forests (Figure 5f). This is caused by the balance between bed accretion and SLR as increased inundation initially relieves the stress in mangrove areas with previously low hydroperiods, allowing mangroves to develop larger biomass (Figure 5f and darker green shades in SLR scenarios in Figure 3).

The change in mangrove forest area and biomass has profound implications for carbon stocks and fluxes. Under the RCP2.6 and RCP4.5 scenarios, total carbon stocks continue to increase, but less than in the no SLR simulation (Figure 5g). The reduction in stored carbon under these scenarios is relatively limited given the considerable reduction in forest area (Figure 5e). This is indeed related to the higher biomass density, and thus higher carbon inputs, in remaining mangrove areas as mentioned above. This can also be observed in Figure 4 as the soil in a large part of the basin contains more carbon under RCP2.6 and RCP4.5 than in the default simulation without SLR (red shades in Figures 4e and 4g). Under RCP8.5, however, carbon stocks stabilize and can even decrease because of negative fluxes, especially under low sediment supply (Figures 5g and 5h). This represents not only the limited production of organic material and ongoing decomposition, but also the erosion of carbon-rich soils and carbon export to the offshore region (Figure 5i). Such export of carbon exists in all scenarios but is accelerated with increasing SLR rates. There is a decline though in C_{soil} export during the final decades of the simulations under RCP8.5, as carbon near the surface and available for erosion becomes limited. As such, the total export of carbon is somewhat comparable at the end of the SLR simulation across all scenarios (Figure 5i).

10.1029/2025EF006984

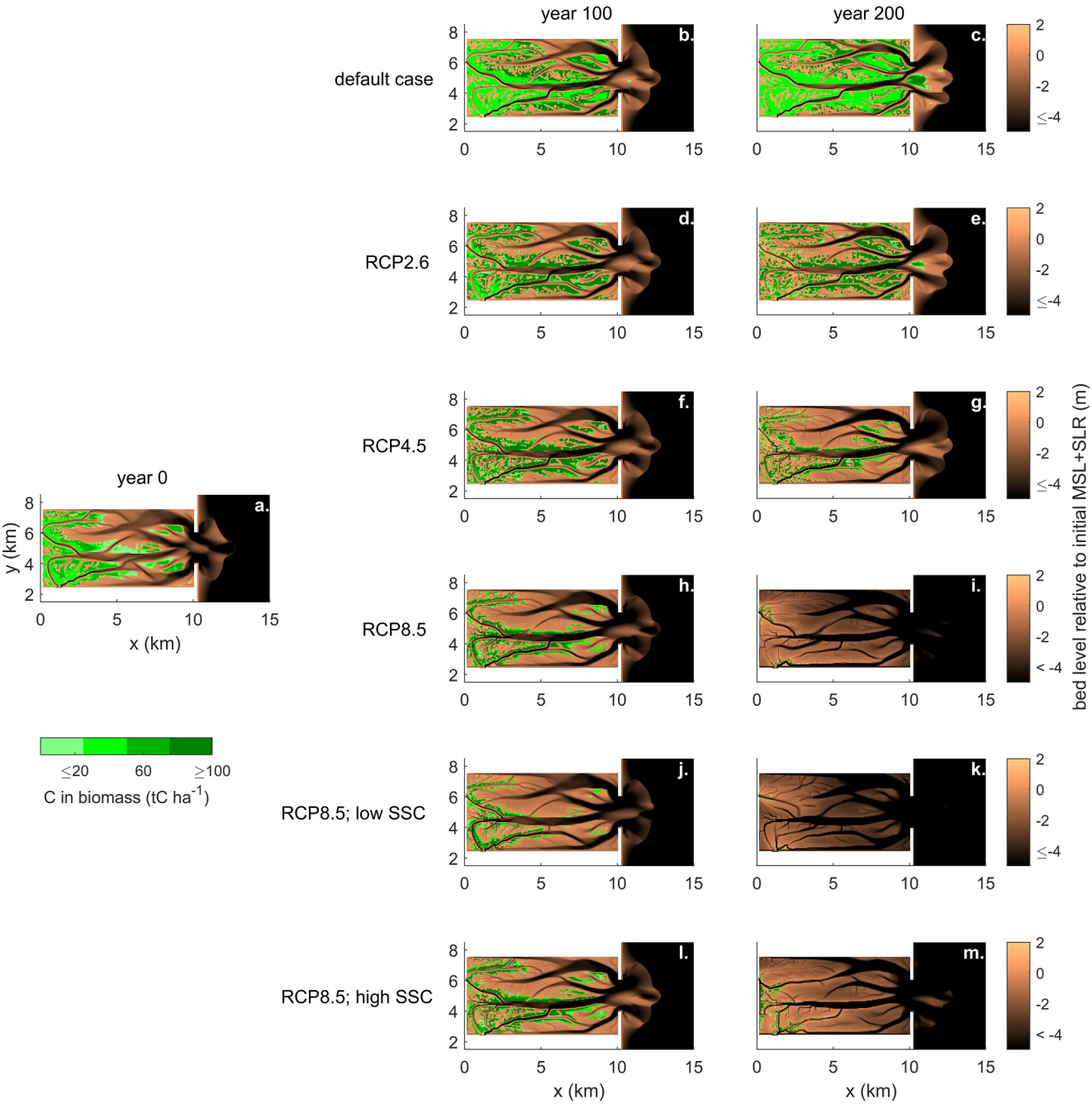

Figure 3. Bed level relative to mean sea level and sea-level rise (SLR), overlaid with carbon content in living biomass (indicated by green color) at different time intervals: before SLR (a), 100 years after SLR (b, d, f, h, j, l), and 200 years after SLR (c, e, g, i, k, m). Cases include the default case (b), (c), RCP2.6 (d), (e), RCP4.5 (f), (g), RCP8.5 (h), (i), RCP8.5 with low suspended sediment concentration (SSC) (j), (k), and RCP8.5 with high SSC (l, m).

3.2. Intra-System Variations

In addition to landscape-scale responses that are strongly controlled by SLR rates and sediment supply, spatial patterns suggest that mangrove growth conditions can be suboptimal near channels, initially resulting in lower biomass (Figures 3a–3c) and carbon accumulation (Figures 4a–4c). However, mangroves near channels can withstand higher SLR rates and survive for longer (Figures 3d–3m), ensuring prolonged carbon inputs (Figures 4d–4m). Overall, the complex landscape development can drive different trajectories of mangrove forests and carbon stocks. Figure 6 shows the morphological evolution and soil carbon contents at different time

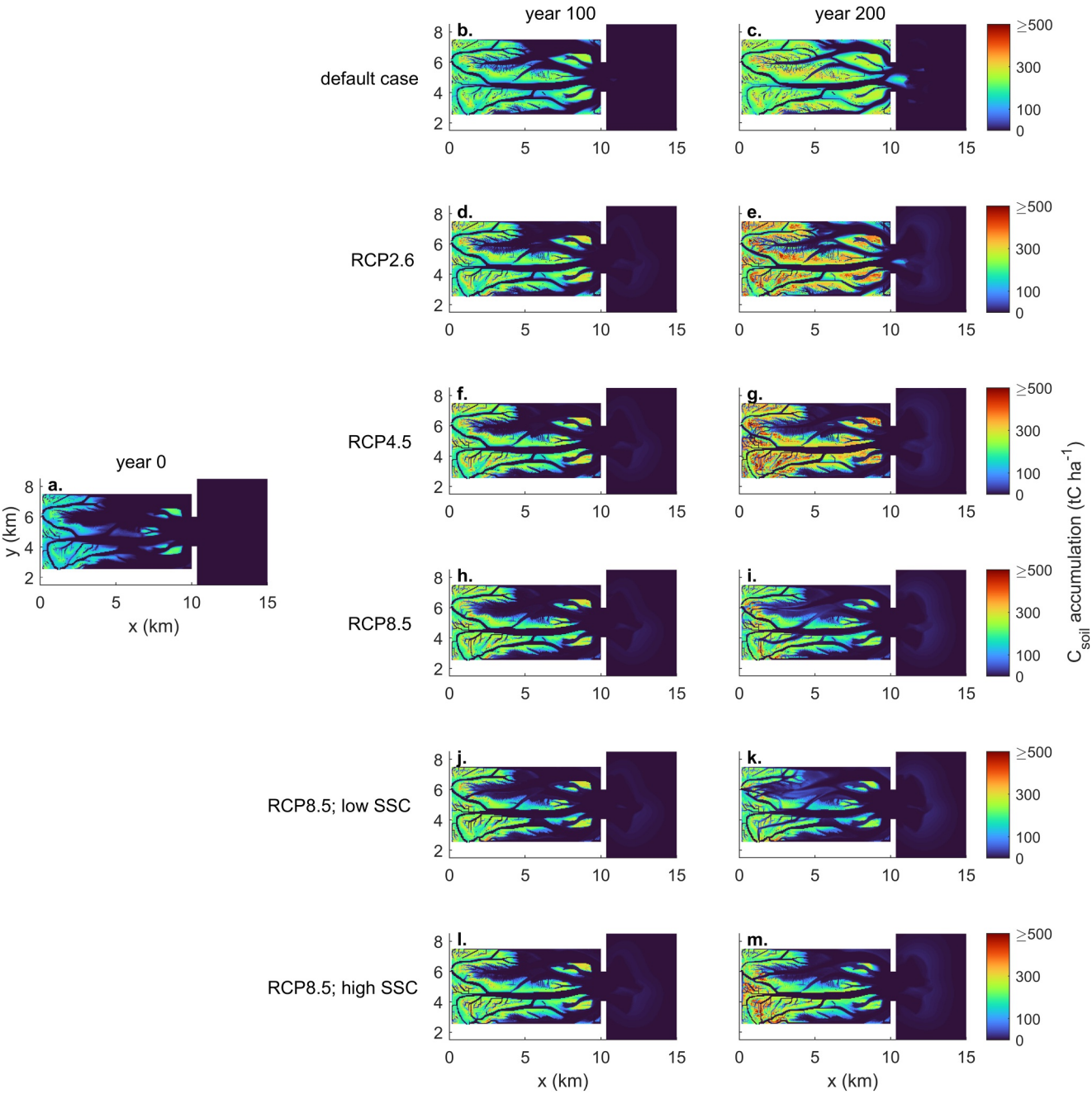

Figure 4. C_{soil} stock at different time intervals and cases, arranged in the same order as Figure 3.

intervals under the RCP8.5 scenario and default SSC. Three distinct behaviors in C_{soil} dynamics occur in response to SLR, which are tightly linked to channel network dynamics.

First, further away from channels at location 1 in Figures 6a–6c, lower rates of bed accretion and high relative SLR drives a rapid increase in hydroperiod surpassing mangrove survival thresholds, ultimately causing mangrove mortality (Figures 6c and 7a). This drowning of mangroves is the most dominant behavior representing the fate of 75% of mangroves within the embayment (Figures 6e and 6f). After mortality, a lack of carbon inputs, deposition of mineral sediment at the surface and ongoing decomposition processes lead to gradual loss C_{soil} stocks (Figure 7c) and burial of previously stored carbon (Figure 7d).

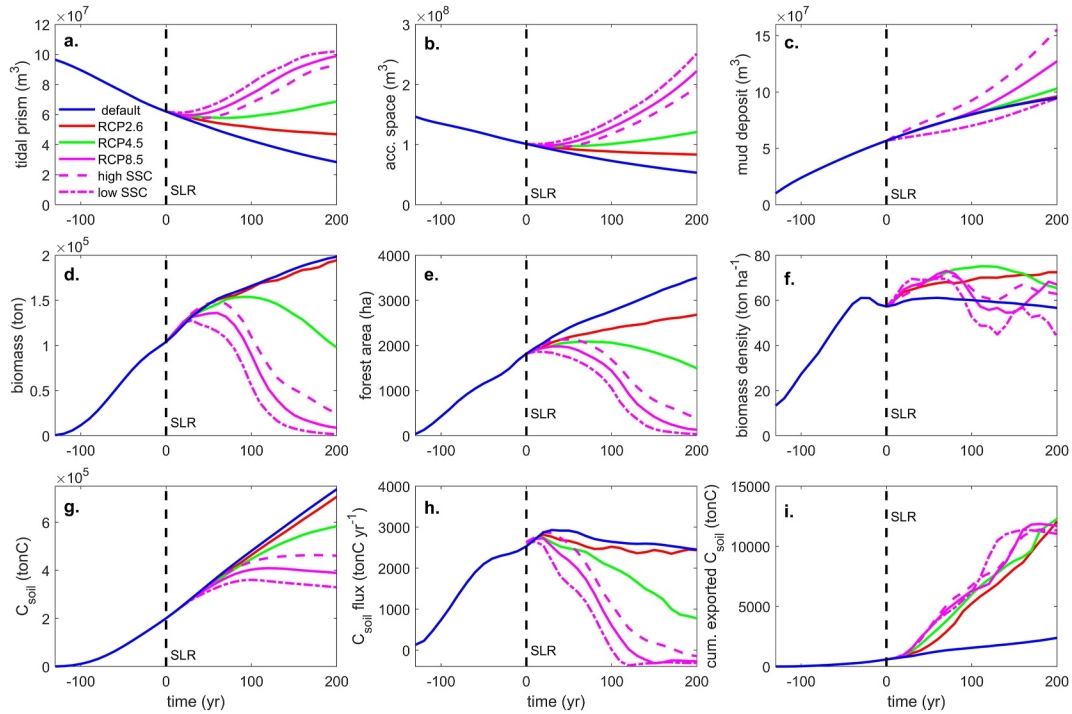

Figure 5. System-wide time series of hydrodynamics, sediment dynamics, forest properties and carbon dynamics for all simulations. Variables include (a) tidal prism, (b) accommodation space for sediment transport, (c) suspended sediment concentration accumulation, (d) total biomass, (e) forest area, (f) biomass density within forest area, (g) C_{soil} stock in embayment, (h) net accumulation of C_{soil} and (i) cumulative export of C_{soil}. The x-axis spans from year −150 to year 200, where the period from −150 to 0 represents the spin-up time.

Second, Location 2 in Figures 6a–6c represents the dynamics in close proximity to channels where the combination of sediment accumulation and SOM production allow mangroves to keep pace with SLR throughout the simulation period. As tidal channels are the main conduits of sediment transport, the large availability and deposits of sediment on channel banks cause the bed elevation to closely track SLR, supporting ongoing mangrove growth (Figures 6a–6c and 7e). Before SLR (year 0), as mangroves are positioned relatively high within the tidal frame close to high water level, mangrove biomass is relatively low because of reduced growth conditions linked to limited hydroperiod (Figures 7e and 7f). At the beginning of SLR, hydroperiods increase, triggering an increase in biomass and soil carbon inputs (Figure 7f). However, as SLR rates continue to increase, the hydroperiod will exceed the optimal value (Figure 7e). This causes a reduction in biomass and C_{soil} inputs during the last 50 years of the simulation (Figure 7f). As a result, despite ongoing mangrove growth, carbon stocks stabilize (Figure 7g) and carbon contents in the top soil layers are decreasing (Figure 7h). Under the RCP8.5 scenario, less than 10% of the initial forest area survives throughout the simulation period (Figures 6e and 6f).

Lastly, Location 3 in Figures 6a–6c exemplifies locations where morphodynamic processes linked to channel dynamics determine C_{soil} changes. Initially, accretion facilitates mangrove survival (Figures 7i and 7j) and C_{soil} accumulation (Figures 7k and 7l), but ongoing increases in hydroperiod results again in mangrove biomass reduction (Figures 7i and 7j). Critically, following mangrove losses, channel formation and erosion of mangrove soils (Figures 6b, 6c and 7i) start to deplete C_{soil}. After approximately 100 years, all previously stored carbon is eroded (Figures 7k and 7l). Under RCP8.5, in about 20% of the area covered with mangroves pre-SLR such erosion of carbon-rich soils occurs (Figure 6f). Although bed elevations may increase after channels have incised (Figures 6a–6c and 7i), because of infilling, channel development fully submerges such locations (Figure 7i; hydroperiod reaches 1).

The importance of channel networks in controlling mangrove and carbon dynamics is further highlighted in Figure 8. An inverse relationship exists between mangrove SLR rate survival thresholds and the lateral distance of forests to the nearest channels. Thus, mangroves located closer to channels can survive longer and withstand

10.1029/2025EF006984

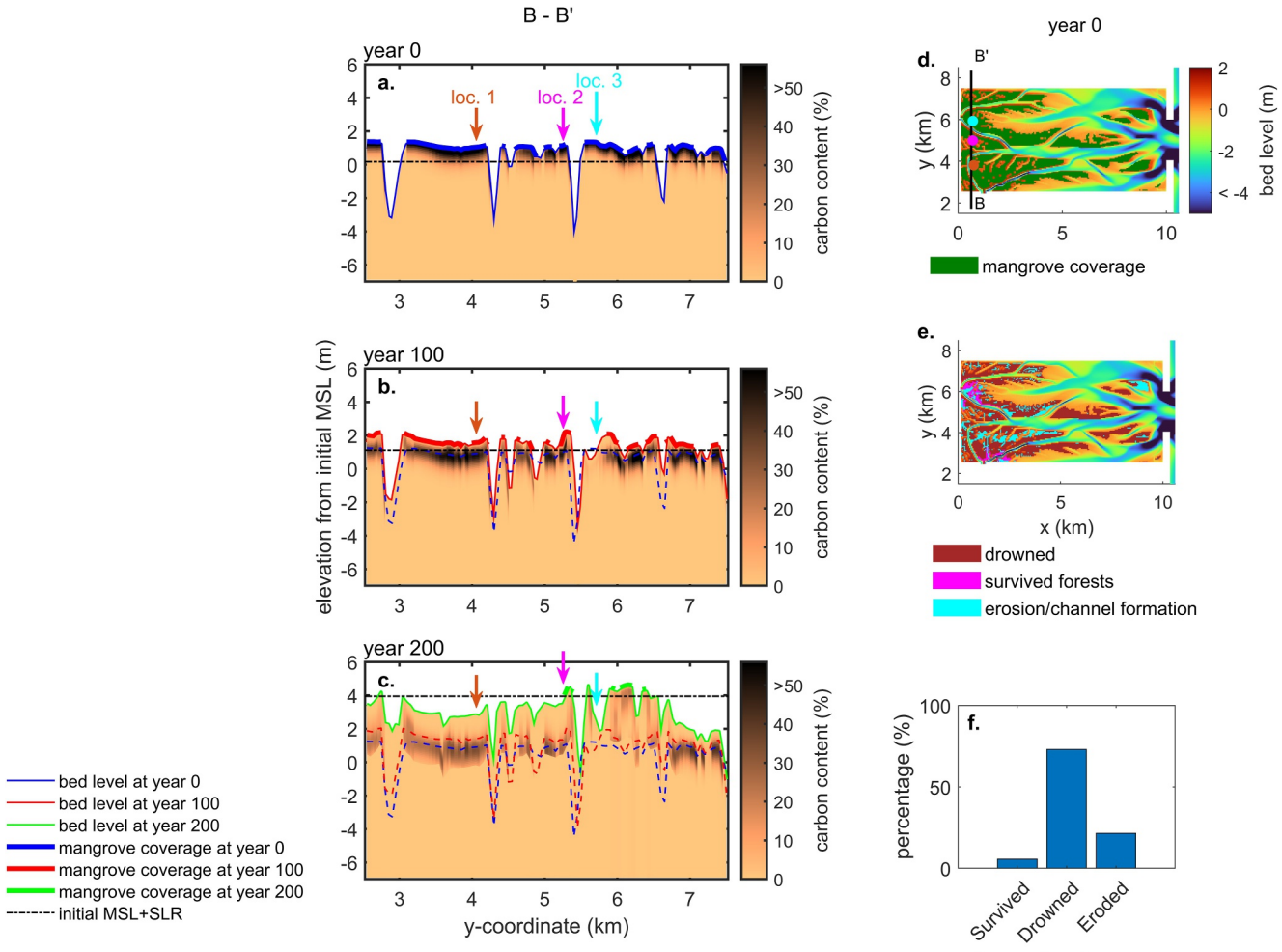

Figure 6. Transect of C_{soil} content over depth across the embayment covered by mangrove forests at three-time intervals: (a) at the beginning of sea-level rise (SLR), (b) 100 years after SLR, and (c) 200 years after SLR for the RCP8.5 scenario with default suspended sediment concentration. The top inset map (panel d) displays the morphology and mangrove forest coverage before SLR, overlayed by transect location with specific highlighted locations (loc. 1, loc. 2, and loc. 3). The bottom inset map (panel e) indicates areas across the embayment that exhibit similar morphological and forest development characteristics as the highlighted locations, represented by shaded colors corresponding to the arrows indicating each location. The relative percentage of each development characteristic is illustrated in the accompanying bar plot (panel f).

higher rates of SLR. Such a relationship applies to mangroves that are either situated in zones influenced by fluvial-dominated or tide-dominated channels. However, highest SLR rate survival thresholds are found for mangroves near fluvial-dominated channels as these are the main sources of sediment (Figure 8a; blue dots for SLR thresholds exceeding 35 mm yr^{-1}).

While mangroves closer to channels are more likely to persist, higher erosion rates of carbon-rich sediments are also found near channels (Figures 8b and 8c). This highlights the role of channel network development, which is triggered by SLR, in depleting carbon stocks. Higher carbon erosion rates are mainly found later in the simulation when SLR rates are accelerating (Figures 8b and 8c; predominantly red, green and black dots for erosion rates exceeding 3 mm/yr). The inverse relationship between distance to the nearest channel and erosion rates is more profound for fluvial-dominated zones, while erosion rates are higher further away from channels under tide-dominated conditions (e.g., exceeds 3 mm yr^{-1} for distances larger than 200 m; Figure 8c). This emphasizes the complexity and spatial variations in carbon dynamics and underlying drivers of erosion processes in particular.

10.1029/2025EF006984

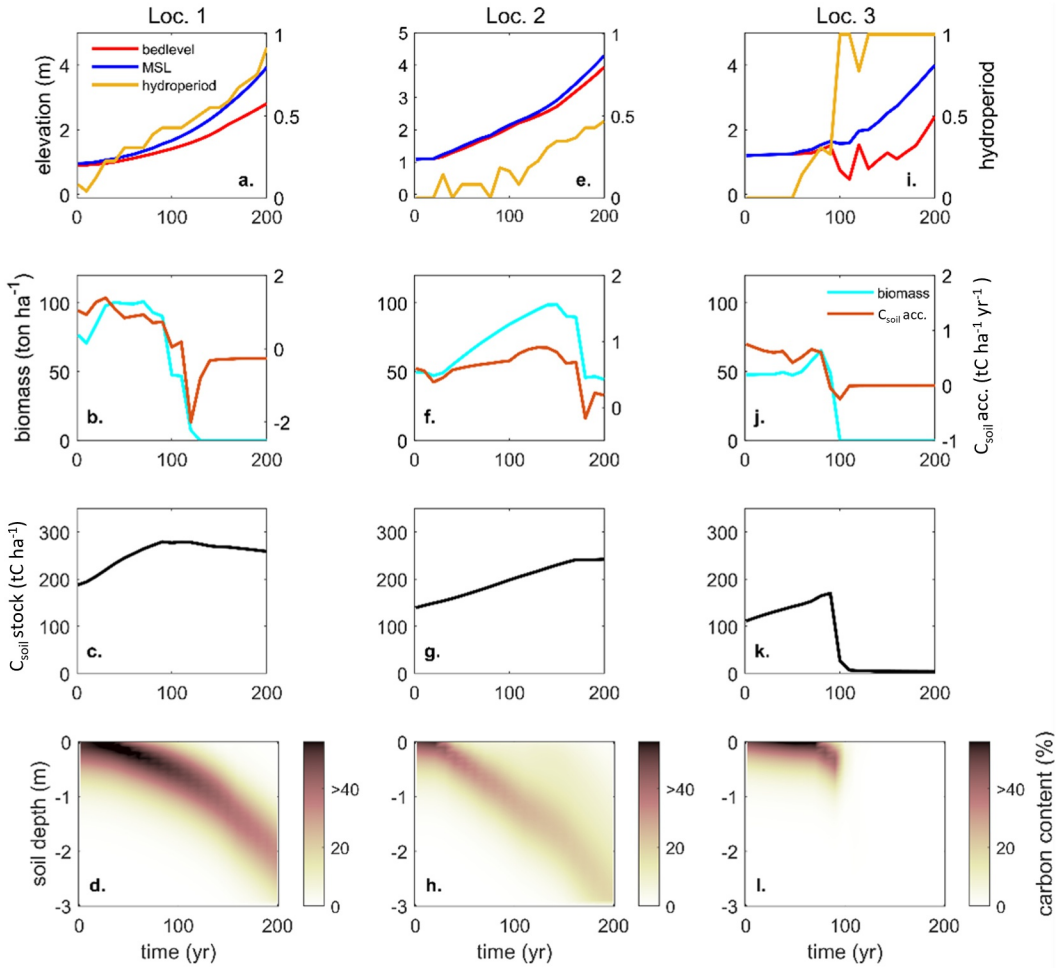

Figure 7. Time series of bed elevation, mean sea level and hydroperiod (a, e, i), biomass and net accumulation of C_{soil} per area, including production, decomposition, erosion and deposition (b, f, j), C_{soil} stock (c, g, k), as well as carbon content over the soil depth (d, h, i) at the same observation points as in Figures 6a–6c.

4. Discussion

4.1. Local-Versus Landscape-Scale Trends

SLR can simultaneously enhance local carbon sequestration in existing mangrove stands while reducing landscape-wide carbon stocks due to limited mangrove expansion. Carbon sequestration in coastal wetlands, including both mangrove and salt marsh ecosystems, has been reported to increase under SLR (e.g., Herbert et al., 2021; Kelleway et al., 2016; Krauss et al., 2017; Rogers et al., 2019; Wang et al., 2019). This suggests that total carbon stocks may increase where wetland vegetation persists, as increased inundation promotes biomass growth and carbon input, at least initially. Our simulations similarly show that SLR enhances soil carbon accumulation in over 98% of existing mangrove areas (Figures 4b–4i and 7b–7k), while rising sea levels cause an immediate reduction in carbon sequestration in only less than 2% of the forest (Table S2 in Supporting Information S1). However, despite this localized gain, SLR has an immediate negative effect on landscape-scale carbon stocks (Figures 5g and 5h), primarily by reducing areas suitable for mangrove colonization (Figure 5e). In contrast, in the absence of SLR, mangroves continue to expand and increase overall carbon storage. Thus, although SLR enhanced carbon sequestration locally in established mangroves, it is outweighed by the negative effects of SLR on habitat development and resulting impacts on carbon stocks at the landscape scale.

These contrasting trends in carbon stocks at local-versus landscape-scales may be more prominent in sediment rich systems where the delivery of sediment allows for the creation of new habitats as accommodation space

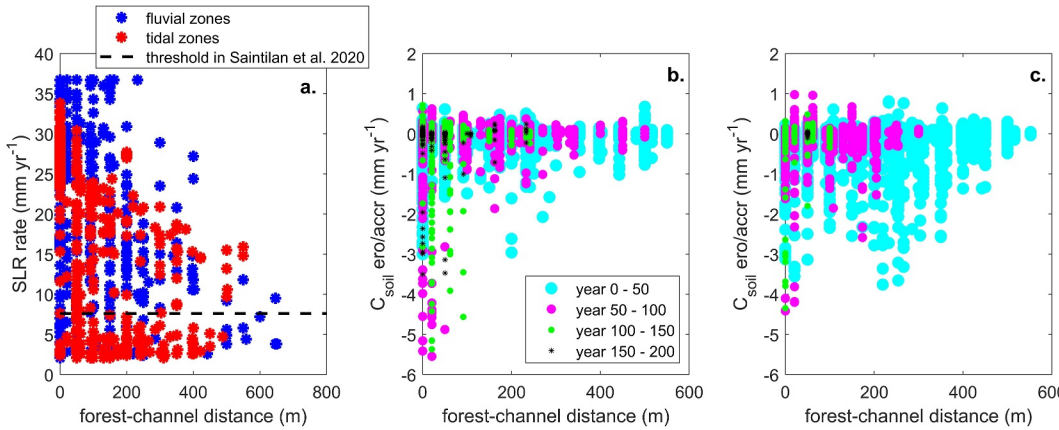

Figure 8. Relationship between key indicators describing mangrove and carbon dynamics as a function of distance to the nearest channels across different hydrodynamic zones within the embayment for the RCP8.5 scenario and default suspended sediment concentration. (a) Mangrove sea-level rise (SLR) rate thresholds in fluvial- and tide-dominated zones (blue and red asterisk, respectively) overlaid by the SLR threshold above which mangroves are unlikely to survive according to Saintilan et al. (2020), and C_{soil} erosion (negative values) and accretion (positive values) rates in (b) fluvial-dominated zones and (c) tide-dominated zones. Fluvial-dominated zones are defined as the channels that always have seaward flow direction within tidal cycle while tide-dominated zones have bi-directional flow conditions.

reduces and bed elevations generally increase while the basin fills in with sediment (Xie et al., 2023). At locations with limited sediment supply, where mangroves rely mainly on organic matter production and lateral eco-morphodynamic processes are less prominent (Mckee et al., 2007), temporal trends of carbon stocks at the landscape-scale may mimic local carbon sequestration trends. Nevertheless, the contrasting trends at different scales revealed here highlight the difficulty in upscaling measurements of local carbon dynamics to landscape-scale carbon stocks for a broad range of systems, especially under ongoing SLR.

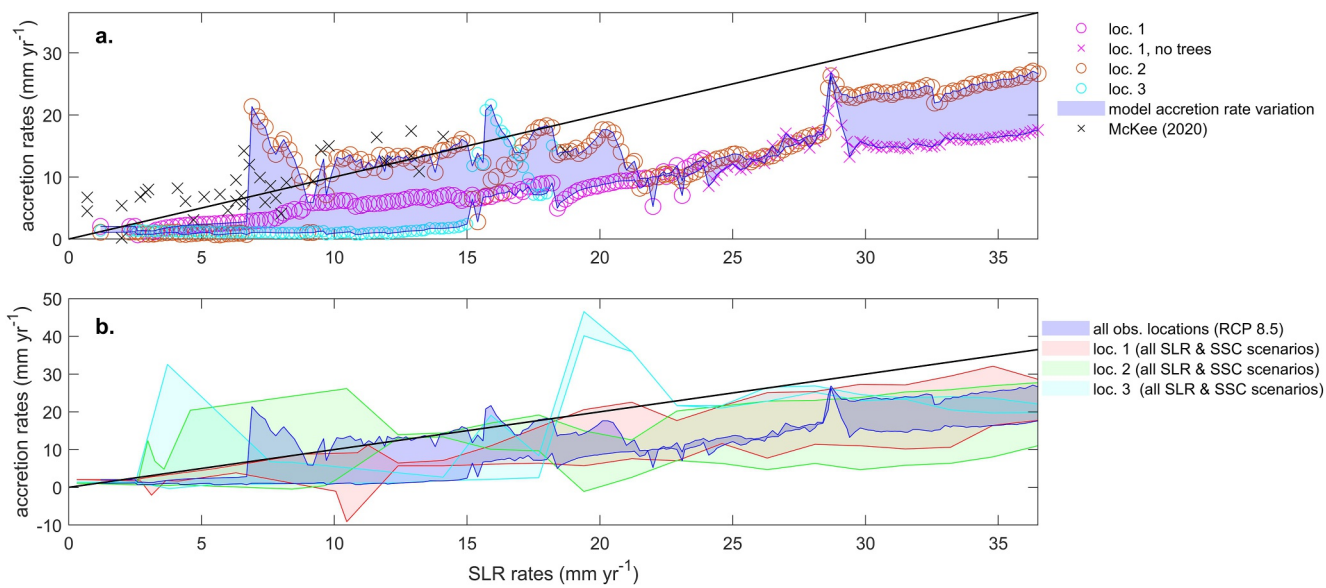

Figure 9. Relationship between sea-level rise (SLR) rates and modeled accretion rates. (a) Modeled accretion rates at specific locations (loc. 1, loc. 2, and loc. 3 in Figure 6) under the RCP8.5 scenario with default suspended sediment concentration compared to empirical data from McKee et al. (2020). The blue shaded area represents the modeled accretion rate variability across the three locations. Transition from circles to crosses for loc. 1 represents tree mortality. The black line indicates the 1:1 relationship between accretion and SLR rates. (b) Accretion rate variability across all locations (blue shaded area; same as in subplot a) in comparison to variability at specific locations across all SLR and sediment supply scenarios, highlighting that the spatial variability linked to eco-morphodynamic processes is in the same order as the variability caused by different external forcing conditions.

4.2. Channel Network Dynamics Control Intra-System Variations

Although carbon sequestration initially increases in the vast majority of the mangrove forest, subsequent mangrove and carbon accumulation trajectories are highly dependent on local geomorphological conditions and channel network dynamics in particular causing intra-system variations. The ability of mangroves to continue sequestering carbon is determined by the SLR thresholds for mangrove survival. Our simulations indicate that these SLR thresholds are a function of the distance between mangroves and the nearest channel (Figure 8a). As channels are the main conduits of sediment transport (Fagherazzi et al., 1999), they control the spatial distribution of sediment across the mangrove forest (Xie et al., 2023). As sediment availability is high in proximity of channels, the accretion rates in these areas are enhanced allowing mangroves to survive higher rates of SLR. Further from channels where sediment availability diminishes, SLR rate survival thresholds are lower, and mangroves are more vulnerable. Consequently, at the intertidal scale, considerable variation exists around the empirically derived relative SLR rate threshold for mangrove survival, as identified by Saintilan et al. (2020) based on data from a broad range of mangrove systems (Figure 8a).

It should be noted though that the process of sediment accumulation in relation to mangrove SLR rate thresholds is rather complex. While sediment accumulation generally increases with SLR, in agreement with field observations, this increase is not linear (Figure 9a). Initially, accumulation is in fact well below the SLR rates for all three locations that represent different mangrove existence and carbon stock trajectories. This would suggest a limited ability of mangroves to keep up with SLR. However, as emphasized previously, an initial deficit in sediment accumulation is a poor guide to evaluate longer term mangrove vulnerability given the highly non-linear dynamics determining bed elevation changes (Kirwan et al., 2016). While an accumulation deficit initially causes increased inundation and lower relative bed elevations, enhanced hydroperiods trigger an acceleration in accretion which enhances mangrove resilience (Krauss et al., 2014; Morris et al., 2023). We observe in our simulations that such increases in accretion can be abrupt and are triggered at different SLR rates for different locations, linked again to the distance from the mangroves to the channel network. As a result of these feedbacks, accretion rates can even exceed SLR rates. Nevertheless, over longer simulation periods with ongoing SLR accelerations, our simulated accretion for these three locations is unable to match SLR rates. Mangroves, however, may still survive for extended periods despite the deficit between accretion and SLR rates. This is caused by mangroves initially being positioned towards the high-tide level and mangroves gradually lowering their relative bed elevation under insufficient accretion but remaining within suitable inundation regimes for several decades (Saintilan et al., 2020; Xie et al., 2022).

While channels and their delivery of sediment play a crucial role in enhancing mangrove resilience under SLR, channel network dynamics are an important driver of carbon loss over longer timescales. SLR is known to enhance channel incision, migration, enlargement and formation because of increases in tidal prism (D'Alpaos et al., 2007; Leuven et al., 2021; Van Maanen et al., 2013). Here we show that such processes can cause the erosion of carbon-rich soils (Figures 6, 7k, 7l, 8b, and 8c) and a transition from a carbon sink to a source (Figure 5g) with carbon being exported to offshore regions (Figure 5i). In nature, once exported, carbon can be redeposited and reburied, repeatedly resuspended and redistributed, or remineralized through microbial decomposition, with the dominant fate controlled by hydrodynamic energy and oxygen exposure both during transport and after offshore deposition (Kristensen et al., 2008). Thus, while previous studies, including modeling studies on C_{soil} dynamics in wetland ecosystems, have mainly highlighted the important role of vertical accretion in maintaining soil elevation to keep pace with SLR (e.g., Kirwan & Mudd, 2012; McKee et al., 2020; Saintilan et al., 2020; Sandi et al., 2021; Woodroffe et al., 2016), our simulations indicate the significant impact of erosional and lateral processes on C_{soil} loss. Ignoring enhanced channel expansion and migration could therefore lead to overestimation of C_{soil} sequestration and accumulation in a coastal system under SLR.

Overall, the strong control of channel network dynamics on mangrove SLR thresholds and carbon erosion suggests distinct drivers of mangrove carbon accumulation at different scales. While SLR and sediment supply (i.e., external drivers) control landscape-scale responses, spatial variations in mangrove and carbon dynamics at the intertidal scale are prominent and determined by internal dynamics linked to the eco-morphodynamics of channel networks. This is further illustrated by Figure 9b, showing that the variability in bed accretion rates, which is crucial for mangrove resilience and carbon sequestration, occurring at single locations across coastal system subject to different SLR and sediment supply scenarios is of the same order as the spatial variation within an individual scenario.

While variations in mangrove and carbon dynamics linked to channel networks and nearby water bodies have been observed in the field, spatial patterns are complex and not necessarily consistent between sites (Hatje et al., 2021; Mizanur Rahman et al., 2015; Owers et al., 2020; Wang et al., 2013). This highlights the complexity of controlling processes of carbon accumulation in coastal systems. Also, comparisons with field studies are challenging because of the typically limited spatial coverage of empirical data. In this context, the observations made in the Venice lagoon in Italy are highly relevant as they allow the systematic analysis of the influence of tidal channel networks on wetland accretion patterns. From a dense network of observational points, it is derived that the inorganic component is crucial near channels while the organic component contributes largely to accretion in the inner marsh. Interestingly, these patterns coincide with vegetation density being lower further away from channels and levees where surface elevation is lower, thus highlighting the potential effects of spatial variations in organic matter decomposition (Puppin et al., 2023; Roner et al., 2016). Therefore, while such studies support our findings of the importance of channel networks in controlling intra-system variations in the balance between organic and inorganic deposition, and thus carbon sequestration rates, they also highlight the complexity and multitude of governing processes in real-world systems.

4.3. Limitations and Future Advancements

This study showed the effects of SLR and sediment supply changes on carbon dynamics in mangrove ecosystems. We intentionally simplified some aspects of boundary and initial conditions as well as process treatment, to facilitate model interpretations and allowing us to focus on eco-carbon-morphodynamic interactions and the role of channel networks. Here we highlight some key model limitations and propose directions for further research linked to boundary conditions, internal parameterizations and process implementations.

The boundary conditions defined in our model simplified complexities of real-world coastal systems. Our model did not include river discharge variations and thus variations in associated sediment supply and subsequent impacts on coastal morphology and ecosystems. River discharge can be affected by seasonal variations, climatic oscillations (e.g., ENSO), climate change and human interventions (Restrepo et al., 2016; Ávila & Gallo, 2021). Also, our model simulations exclude inputs of allochthonous carbon from catchment areas. While mangrove-derived autochthonous carbon is typically known to be the dominant contributor (Saintilan et al., 2013; Zhang et al., 2024), allochthonous inputs may be important for some systems (Mcleod et al., 2011; Rosentreter et al., 2018; Volta et al., 2020). Not including such inputs could therefore result in an underestimation of simulated carbon storage as well as affect spatial and temporal patterns of carbon capture as allochthonous carbon is likely to be captured close to channels and is enhanced under SLR (Suello et al., 2025). As this study focuses on long-term dynamics of autochthonous carbon as the main source of mangrove soil carbon, boundary conditions are simplified but the model can be further developed and utilized to examine the variability of river discharge and the response of allochthonous carbon sink dynamics to future threats such as climate change and increasing human activities.

Model parameterization of organic matter production and decomposition processes, despite based on current understanding, may not capture the full complexity of these processes. While our model addresses how changes in inundation impact mangrove growth, and thus biomass and organic matter production, we did not include the impact of enhanced flooding on, for example, root production, as it is hard to predict and parameterize (Krauss et al., 2014). Additionally, higher water levels can lead to more anaerobic conditions, potentially slowing decomposition rates (Mckee et al., 2007; Wolf et al., 2007). Incorporating such feedbacks would result in larger carbon stocks in our SLR scenarios. However, in some cases, increased inundation has also been found to have little effect or can even enhance decomposition (Arnaud et al., 2020; Kirwan et al., 2013), such that net effects may be highly site dependent. Vertical variability in decomposition throughout the soil column may also exist. The top layers of mangrove soils typically have higher decomposition rates due to higher oxygen availability, while decomposition rates generally decrease as depth increases (Kristensen et al., 2008). SLR can alter these depth-dependent decomposition patterns by increasing water table levels, potentially creating more anaerobic conditions at shallower soil depths (Arnaud et al., 2020). Implementing such processes can open exiting opportunities for new model development and coupling of vegetation and groundwater models (Peters et al., 2020).

Mangrove growth and thus biomass patterns in the model here are only influenced by inundation regimes, following other theoretical and modeling work (Krauss et al., 2008; Morris et al., 2023; Xie et al., 2020). However, in natural systems, other factors can contribute to intra-system variation of mangrove biomass and

carbon stocks. For example, nutrient availability and salinity can influence mangrove productivity and carbon sequestration (Krauss et al., 2014; Reef et al., 2010). At the same time, the transport of nutrients and saline water is influenced by fluvial and tidal processes and thus tightly linked to geomorphological setting and channel network characteristics (Adame et al., 2010). Our modeling study here shows how channel networks have a strong control on carbon accumulation merely through their effect on spatial variations in mineral sediment availability and deposition, morphological development and inundation regimes, which in turn affect mangrove biomass development. Incorporating additional factors, such as nutrient availability and salinity, is likely to further enhance the intra-system variability of mangrove carbon stocks and dynamics. While such model developments would also allow for more detailed model-data comparisons, it will also complicate the interpretation of complex eco-carbon-morphodynamic interactions.

Lastly, while our simulations offer valuable insights into the response of mangrove ecosystems to SLR, their applicability to natural systems should consider the assumption of monospecific forest composition. In natural systems, mangrove ecosystems are often composed of multiple coexisting species—such as *Rhizophora* spp., *Laguncularia spp*., *Sonneratia* spp., and *Aegiceras spp*.—each with distinct tolerances to inundation, salinity, and sediment dynamics (Berger et al., 2006). These species assemblages form structurally and functionally diverse communities where interspecific interactions, such as facilitation or competition, can influence forest development, carbon accumulation, and resilience to disturbance (Berger et al., 2006; Berger & Hildenbrandt, 2000). Furthermore, the inclusion of other key ecological processes with a critical role in forest regeneration and landward migration in response to SLR (e.g., herbivory, propagule production, predation, and dispersion) (Berger et al., 2008; Porté & Bartelink, 2002; Wei et al., 2024), could enhance model's capacity to fully unravel the complexity of mangrove responses to environmental change at different scales.

4.4. Broader Implications for Blue Carbon Assessment

The increased recognition of mangroves as blue carbon hotspots has resulted in important progress on monitoring protocols and improved data of mangrove blue carbon around the world (Kauffman & Donato, 2012). At the same time, it has been highlighted that estimates at a site cannot be upscaled to regional scale if the drivers of carbon sequestration are different or unknown (Saintilan et al., 2013). Here we show that, apart from the challenge in upscaling to regional scales, even upscaling local observations of carbon dynamics across a broader mangrove landscape is uncertain, given the strong intra-system variations in carbon accumulation processes and the divergence of carbon stock trajectories which is likely to be reinforced under SLR. Blue carbon assessment must evolve to incorporate the spatial and temporal variability of morphological development and mangrove forest dynamics. Global- and country-scale assessment methods often rely on average estimates and extrapolations (Kauffman & Donato, 2012; Wang et al., 2025), which potentially overlook the complexities and possible wide range of carbon stock variations within the system (Hapsari et al., 2024; Kusumaningtyas et al., 2019; Mizanur Rahman et al., 2015). A more accurate carbon stock assessment and estimation of temporal changes could be achieved by integrating eco-carbon-morphodynamic modeling as performed in this study and high-resolution data combined with novel analysis techniques (Sanderman et al., 2018; Sharma et al., 2022; Wicaksono et al., 2016). By improving the carbon stock estimation practices, effectiveness of blue carbon accounting in policy frameworks and carbon market mechanisms can be enhanced.

5. Conclusions

We developed an eco-carbon-morphodynamic model capable of capturing mutual feedback between hydro-morphodynamic processes, mangrove forest dynamics and soil carbon dynamics. This model was utilized to investigate the effects of SLR and changes in sediment supply on mangrove carbon dynamics. A schematized tidal embayment was set up, and a series of simulations were conducted under varying scenarios of SLR and fluvial sediment availability. Our findings highlight the scale-dependency of carbon accumulation responses and controlling drivers.

Locally, SLR triggers enhanced carbon accumulation, because increased inundation promotes biomass growth and carbon inputs. However, at the landscape-scale, SLR has a direct negative impact on carbon storage as it limits development of new mangrove areas. As SLR continues to accelerate, mangrove mortality, ongoing decomposition and erosion of carbon-rich soils reduce potential soil carbon accumulation and increase the export of soil carbon offshore. This implies that at the landscape scale, SLR could cause mangrove ecosystem to change

from a net soil-carbon sink to a source (C_{soil} loss), highlighting the vulnerability and impermanence of blue carbon systems.

At the intertidal-scale, strong spatial variations in carbon accumulation trajectories exist which are controlled by channel network dynamics and sedimentation patterns. Mangroves in proximity of channels exhibit higher SLR rate thresholds for survival, such that prolonged carbon accumulation is ensured. At the same time, as increases in tidal prism cause channel expansion, channel network dynamics play a crucial role in the erosion of carbon-rich soils and carbon export.

Clearly, distinct drivers determine mangrove carbon accumulation at different scales with internal system dynamics shown to be equally important as external forcings. Given the complexity of drivers and contrasting trends in carbon dynamics at different spatial and temporal scales, local observations of carbon accumulation do not necessarily reflect longer-term landscape-wide carbon stocks. Overall, our study highlights the importance of scale for understanding blue carbon dynamics in mangroves under different SLR scenarios and the complex eco-carbon-morphodynamic interactions that need to be considered when evaluating mangrove potential for climate change mitigation in the future.

Conflict of Interest

The authors declare no conflicts of interest relevant to this study.

Availability Statement

The eco-carbon-morphodynamic model source code developed in this study is archived in Zenodo (Iwantoro et al., 2026) (https://doi.org/10.5281/zenodo.18926971) and is also publicly available at github.com/aryaiwantoro/Carbongroove. The model was developed and implemented within the Delft3D (version 4.01.00) (Lesser et al., 2004) and MATLAB (version R2022b) environment.

Acknowledgments
This research was part of the "Mangrove ecosystem services under pressure: the history and future of carbon sequestration hotspots" project, supported by the Natural Environment Research Council (NERC, NE/V012800/1), which is part of UK Research and Innovation.

References

Adame, M. F., Virdis, B., & Lovelock, C. E. (2010). Effect of geomorphological setting and rainfall on nutrient exchange in mangroves during tidal inundation. *Marine and Freshwater Research*, *61*(10), 1197–1206. https://doi.org/10.1071/MF10013

Alongi, D. M. (2011). Carbon payments for mangrove conservation: Ecosystem constraints and uncertainties of sequestration potential. *Environmental Science & Policy*, *14*(4), 462–470. https://doi.org/10.1016/j.envsci.2011.02.004

Alongi, D. M. (2012). Carbon sequestration in mangrove forests. In *Carbon Management* (Vol. 3 (Iss. 3), pp. 313–322). https://doi.org/10.4155/cmt.12.20

Alongi, D. M. (2014). Carbon cycling and storage in mangrove forests. *Annual Review of Marine Science*, *6*(1), 195–219. https://doi.org/10.1146/annurev-marine-010213-135020

Alongi, D. M. (2021). Responses of mangrove ecosystems to climate change in the anthropocene. In *Mangroves: Ecology, biodiversity and management*. https://doi.org/10.1007/978-981-16-2494-0_9

Alongi, D. M. (2022). Impacts of climate change on blue carbon stocks and fluxes in mangrove forests. *Forests*, *13*(2), 149. https://doi.org/10.3390/f13020149

Arnaud, M., Baird, A. J., Morris, P. J., Dang, T. H., & Nguyen, T. T. (2020). Sensitivity of mangrove soil organic matter decay to warming and sea level change. *Global Change Biology*, *26*(3), 1899–1907. https://doi.org/10.1111/gcb.14931

Ávila, B., & Gallo, M. N. (2021). Morphological behavior of the Magdalena River delta (Colombia) due to intra and interannual variations in river discharge. *Journal of South American Earth Sciences*, *108*, 103215. https://doi.org/10.1016/j.jsames.2021.103215

Balke, T., Bouma, T. J., Horstman, E. M., Webb, E. L., Erftemeijer, P. L. A., & Herman, P. M. J. (2011). Windows of opportunity: Thresholds to mangrove seedling establishment on tidal flats. *Marine Ecology Progress Series*, *440*, 1–9. https://doi.org/10.3354/meps09364

Baptist, M. J., Babovic, V., Uthurburu, J. R., Keijzer, M., Uittenbogaard, R. E., Mynett, A., & Verwey, A. (2007). On inducing equations for vegetation resistance. *Journal of Hydraulic Research*, *45*(4), 435–450. https://doi.org/10.1080/00221686.2007.9521778

Benner, R., Hatcher, P. G., & Hedges, J. I. (1990). Early diagenesis of mangrove leaves in a tropical estuary: Bulk chemical characterization using solid-state 13C NMR and elemental analyses. *Geochimica et Cosmochimica Acta*, *54*(7), 2003–2013. https://doi.org/10.1016/0016-7037(90)90268-P

Berger, U., Adams, M., Grimm, V., & Hildenbrandt, H. (2006). Modelling secondary succession of neotropical mangroves: Causes and consequences of growth reduction in pioneer species. *Perspectives in Plant Ecology, Evolution and Systematics*, *7*(4), 243–252. https://doi.org/10.1016/j.ppees.2005.08.001

Berger, U., & Hildenbrandt, H. (2000). A new approach to spatially explicit modelling of forest dynamics: Spacing, ageing and neighbourhood competition of mangrove trees. *Ecological Modelling*, *132*(3), 287–302. https://doi.org/10.1016/S0304-3800(00)00298-2

Berger, U., Rivera-Monroy, V. H., Doyle, T. W., Dahdouh-Guebas, F., Duke, N. C., Fontalvo-Herazo, M. L., et al. (2008). Advances and limitations of individual-based models to analyze and predict dynamics of mangrove forests: A review. *Aquatic Botany*, *89*(2), 260–274. https://doi.org/10.1016/j.aquabot.2007.12.015

Beselly, S. M., Grueters, U., van Der Wegen, M., Reyns, J., Dijkstra, J., & Roelvink, D. (2023). Modelling mangrove-mudflat dynamics with a coupled individual-based-hydro-morphodynamic model. *Environmental Modelling and Software*, *169*, 105814. https://doi.org/10.1016/j.envsoft.2023.105814

Black, K. S., Tolhurst, T. J., Paterson, D. M., & Hagerthey, S. E. (2002). Working with natural cohesive sediments. *Journal of Hydraulic Engineering*, *128*(1), 2–8. https://doi.org/10.1061/(asce)0733-9429(2002)128:1(2)

Boechat Albernaz, M., Brückner, M. Z. M., van Maanen, B., van der Spek, A. J. F., & Kleinhans, M. G. (2023). Vegetation reconfigures barrier coasts and affects tidal Basin infilling under Sea level rise. *Journal of Geophysical Research: Earth Surface*, *128*(4), e2022JF006703. https://doi.org/10.1029/2022JF006703

Boechat Albernaz, M., Roelofs, L., Pierik, H. J., & Kleinhans, M. G. (2020). Natural levee evolution in vegetated fluvial-tidal environments. *Earth Surface Processes and Landforms*, *45*(15), 3824–3841. https://doi.org/10.1002/esp.5003

Braat, L., Van Kessel, T., Leuven, J. R. F. W., & Kleinhans, M. G. (2017). Effects of mud supply on large-scale estuary morphology and development over centuries to millennia. *Earth Surface Dynamics*, *5*(4), 617–652. https://doi.org/10.5194/esurf-5-617-2017

Breithaupt, J. L., Steinmuller, H. E., Rovai, A. S., Engelbert, K. M., Smoak, J. M., Chambers, L. G., et al. (2023). An improved framework for estimating organic carbon content of mangrove soils using loss-on-ignition and coastal environmental setting. *Wetlands*, *43*(6), 57. https://doi.org/10.1007/s13157-023-01698-z

Brückner, M. Z. M., Schwarz, C., van Dijk, W. M., van Oorschot, M., Douma, H., & Kleinhans, M. G. (2019). Salt marsh establishment and eco-engineering effects in dynamic estuaries determined by species growth and mortality. *Journal of Geophysical Research: Earth Surface*, *124*(12), 2962–2986. https://doi.org/10.1029/2019JF005092

Buffington, K. J., Carr, J. A., MacKenzie, R. A., Apwong, M., Krauss, K. W., & Thorne, K. M. (2024). Projecting mangrove Forest resilience to sea-level rise on a Pacific Island: Species dynamics and ecological thresholds. *Estuaries and Coasts*, *47*(8), 2174–2189. https://doi.org/10.1007/s12237-024-01422-y

Cavanaugh, K. C., Dangremond, E. M., Doughty, C. L., Park Williams, A., Parker, J. D., Hayes, M. A., et al. (2019). Climate-driven regime shifts in a mangrove–salt marsh ecotone over the past 250 years. *Proceedings of the National Academy of Sciences of the United States of America*, *116*(43), 21602–21608. https://doi.org/10.1073/pnas.1902181116

Chen, R., & Twilley, R. R. (1999). A simulation model of organic matter and nutrient accumulation in mangrove wetland soils. *Biogeochemistry*, *44*(1), 93–118. https://doi.org/10.1023/A:1006076405557

D'Alpaos, A., Lanzoni, S., Marani, M., & Rinaldo, A. (2007). Landscape evolution in tidal embayments: Modeling the interplay of erosion, sedimentation, and vegetation dynamics. *Journal of Geophysical Research*, *112*(1), F01008. https://doi.org/10.1029/2006JF000537

Day, J. W., Boesch, D. F., Clairain, E. J., Kemp, G. P., Laska, S. D., Mitsch, W. J., et al. (2007). Restoration of the Mississippi Delta: Lessons from hurricanes Katrina and Rita. *Science*, *315*(Number 5819), 1679–1684. https://doi.org/10.1126/science.1137030

Dissanayake, D. M. P. K., Wurpts, A., Miani, M., Knaack, H., Niemeyer, H. D., & Roelvink, J. A. (2012). Modelling morphodynamic response of a tidal basin to an anthropogenic effect: Ley Bay, East Frisian Wadden Sea - Applying tidal forcing only and different sediment fractions. *Coastal Engineering*, *67*, 14–28. https://doi.org/10.1016/j.coastaleng.2012.04.001

Donato, D. C., Kauffman, J. B., Murdiyarso, D., Kurnianto, S., Stidham, M., & Kanninen, M. (2011). Mangroves among the most carbon-rich forests in the tropics. *Nature Geoscience*, *4*(5), 293–297. https://doi.org/10.1038/ngeo1123

Duarte, C. M., Losada, I. J., Hendriks, I. E., Mazarrasa, I., & Marbà, N. (2013). The role of coastal plant communities for climate change mitigation and adaptation. In *Nature climate change* (Vol. 3, (Iss. 11), pp. 961–968). https://doi.org/10.1038/nclimate1970

Dürr, H. H., Laruelle, G. G., van Kempen, C. M., Slomp, C. P., Meybeck, M., & Middelkoop, H. (2011). Worldwide typology of Nearshore coastal systems: Defining the estuarine filter of River inputs to the Oceans. *Estuaries and Coasts*, *34*(3), 441–458. https://doi.org/10.1007/s12237-011-9381-y

Ellis, J., Nicholls, P., Craggs, R., Hofstra, D., & Hewitt, J. (2004). Effects of terrigenous sedimentation on mangrove physiology and associated macrobenthic communities. *Marine Ecology Progress Series*, *270*, 71–82. https://doi.org/10.3354/meps270071

Ellison, J. C. (1999). Impacts of sediment burial on mangroves. *Marine Pollution Bulletin*, *37*(8–12), 420–426. https://doi.org/10.1016/S0025-326X(98)00122-2

Engelund, F., & Hansen, E. (1967). A monograph on sediment transport in alluvial streams. *Monografia*, *65*. https://doi.org/10.1007/s13398-014-0173-7.2

Fagherazzi, S., Bortoluzzi, A., Dietrich, W. E., Adami, A., Lanzoni, S., Marani, M., & Rinaldo, A. (1999). Tidal networks 1. Automatic network extraction and preliminary scaling features from digital terrain maps. *Water Resources Research*, *35*(12), 3891–3904. https://doi.org/10.1029/1999WR900236

Fox-Kemper, B., Hewitt, H. T., Xiao, C., Aðalgeirsdóttir, G., Drijfhout, S. S., Edwards, T. L., et al. (2021). Ocean, cryosphere and sea level change. In V. Masson-Delmotte, P. Zhai, A. Pirani, S. L. Connors, C. Péan, S. Berger, et al. (Eds.), *Climate change 2021: The physical science Basis. Contribution of Working Group I to the sixth assessment report of the intergovernmental Panel on climate change* (pp. 1211–1362). Cambridge University Press.

Friess, D. A., Krauss, K. W., Horstman, E. M., Balke, T., Bouma, T. J., Galli, D., & Webb, E. L. (2012). Are all intertidal wetlands naturally created equal? Bottlenecks, thresholds and knowledge gaps to mangrove and saltmarsh ecosystems. *Biological Reviews*, *87*(2), 346–366. https://doi.org/10.1111/j.1469-185X.2011.00198.x

Hapsari, K. A., Borrero Avellaneda, W. J., van Maanen, B., Restrepo, J. C., Polanía, J., Sibaja Castillo, D. J., et al. (2024). Structure and carbon stocks of accessible mangroves under different conservation status in the Colombian Caribbean. *Forest Ecology and Management*, *564*, 121984. https://doi.org/10.1016/j.foreco.2024.121984

Hatje, V., Masqué, P., Patire, V. F., Dórea, A., & Barros, F. (2021). Blue carbon stocks, accumulation rates, and associated spatial variability in Brazilian mangroves. *Limnology and Oceanography*, *66*(2), 321–334. https://doi.org/10.1002/lno.11607

Herbert, E. R., Windham-Myers, L., & Kirwan, M. L. (2021). Sea-level rise enhances carbon accumulation in United States tidal wetlands. *One Earth*, *4*(3), 425–433. https://doi.org/10.1016/j.oneear.2021.02.011

Howard, J., Hoyt, S., Isensee, K., Pidgeon, E., & Telszewski, M. (2014). *Coastal blue carbon: Methods for assessing carbon stocks and emissions factors in mangroves, tidal salt marshes, and seagrass meadows*. Conservation International, Intergovernmental Oceanographic Commission of UNESCO, International Union for Conservation of Nature.

IPCC. (2013). *Climate change 2013: The physical science basis. Contribution of Working Group I to the Fifth Assessment Report of the Intergovernmental Panel on climate Change*. Cambridge University Press.1535.

Iwantoro, A. P., Urrego, D. H., Xie, D., Nicholas, A. P., Hapsari, K. A., Rodríguez-Rodríguez, J. A., et al. (2026). Eco-carbon-morphodynamic model for Mangrove systems (Carbongroove) (carbongroove_V1) [software]. *Zenodo*. https://doi.org/10.5281/zenodo.18926971

Jaramillo, V. J., Kauffman, J. B., Rentería-Rodríguez, L., Cummings, D. L., & Ellingson, L. J. (2003). Biomass, carbon, and nitrogen pools in Mexican tropical dry Forest landscapes. *Ecosystems*, *6*(7), 609–629. https://doi.org/10.1007/s10021-002-0195-4

Jervey, M. T. (1988). Quantitative geological modeling of siliciclastic rock sequences and their seismic expression. In *Sea-Level changes: An integrated approach*. https://doi.org/10.2110/pec.88.01.0047

Kauffman, J. B., & Donato, D. C. (2012). *Protocols for the measurement, monitoring and reporting of structure, biomass and carbon stocks in mangrove forests*. CIFOR.

Kelleway, J. J., Saintilan, N., Macreadie, P. I., Skilbeck, C. G., Zawadzki, A., & Ralph, P. J. (2016). Seventy years of continuous encroachment substantially increases "blue carbon" capacity as mangroves replace intertidal salt marshes. *Global Change Biology*, *22*(3), 1097–1109. https://doi.org/10.1111/gcb.13158

Kirwan, M. L., Guntenspergen, G. R., D'Alpaos, A., Morris, J. T., Mudd, S. M., & Temmerman, S. (2010). Limits on the adaptability of coastal marshes to rising sea level. *Geophysical Research Letters*, *37*(23). https://doi.org/10.1029/2010GL045489

Kirwan, M. L., Langley, J. A., Guntenspergen, G. R., & Megonigal, J. P. (2013). The impact of sea-level rise on organic matter decay rates in Chesapeake Bay brackish tidal marshes. *Biogeosciences*, *10*(3), 1869–1876. https://doi.org/10.5194/bg-10-1869-2013

Kirwan, M. L., & Megonigal, J. P. (2013). Tidal wetland stability in the face of human impacts and sea-level rise. *Nature*, *504*(Number 7478), 53–60. https://doi.org/10.1038/nature12856

Kirwan, M. L., & Mudd, S. M. (2012). Response of salt-marsh carbon accumulation to climate change. *Nature*, *489*(7417), 550–553. https://doi.org/10.1038/nature11440

Kirwan, M. L., Temmerman, S., Skeehan, E. E., Guntenspergen, G. R., & Fagherazzi, S. (2016). Overestimation of marsh vulnerability to sea level rise. *Nature Climate Change*, *6*(Number 3), 253–260. https://doi.org/10.1038/nclimate2909

Komiyama, A. (1989). A quantitative analysis of root system of mangrove tree species in Iriomote Island, southern Japan. *Galaxea*, *8*, 89–96.

Krauss, K. W., Cahoon, D. R., Allen, J. A., Ewel, K. C., Lynch, J. C., & Cormier, N. (2010). Surface elevation change and susceptibility of different mangrove zones to sea-level rise on Pacific high islands of Micronesia. *Ecosystems*, *13*(1), 129–143. https://doi.org/10.1007/s10021-009-9307-8

Krauss, K. W., Cormier, N., Osland, M. J., & Kirwan, M. L. (2017). Created mangrove wetlands store belowground carbon and surface elevation change enables them to adjust to sea-level rise. *Scientific Reports*.

Krauss, K. W., Lovelock, C. E., McKee, K. L., López-Hoffman, L., Ewe, S. M. L., & Sousa, W. P. (2008). Environmental drivers in mangrove establishment and early development: A review. *Aquatic Botany*, *89*(Number 2), 105–127. https://doi.org/10.1016/j.aquabot.2007.12.014

Krauss, K. W., Mckee, K. L., Lovelock, C. E., Cahoon, D. R., Saintilan, N., Reef, R., & Chen, L. (2014). How mangrove forests adjust to rising sea level. *New Phytologist*, *202*(Number 1), 19–34. https://doi.org/10.1111/nph.12605

Kristensen, E., Bouillon, S., Dittmar, T., & Marchand, C. (2008). Organic carbon dynamics in mangrove ecosystems: A review. *Aquatic Botany*, *89*(Number 2), 201–219. https://doi.org/10.1016/j.aquabot.2007.12.005

Kusumaningtyas, M. A., Hutahaean, A. A., Fischer, H. W., Pérez-Mayo, M., Ransby, D., & Jennerjahn, T. C. (2019). Variability in the organic carbon stocks, sources, and accumulation rates of Indonesian mangrove ecosystems. *Estuarine, Coastal and Shelf Science*, *218*, 310–323. https://doi.org/10.1016/j.ecss.2018.12.007

Lamont, K., Saintilan, N., Kelleway, J. J., Mazumder, D., & Zawadzki, A. (2020). Thirty-Year repeat measures of mangrove Above- and below-ground biomass reveals unexpectedly high carbon sequestration. *Ecosystems*, *23*(2), 370–382. https://doi.org/10.1007/s10021-019-00408-3

Lesser, G. R., Roelvink, J., van Kester, J. T. M., & Stelling, G. S. (2004). Development and validation of a three-dimensional morphological model. *Coastal Engineering*, *51*(8–9), 883–915. https://doi.org/10.1016/j.coastaleng.2004.07.014

Leuven, J. R. F. W., van Keulen, D., Nienhuis, J. H., Canestrelli, A., & Hoitink, A. J. F. (2021). Large-Scale scour in response to tidal dominance in estuaries. *Journal of Geophysical Research: Earth Surface*, *126*(5), e2020JF006048. https://doi.org/10.1029/2020JF006048

Lovelock, C. E., Cahoon, D. R., Friess, D. A., Guntenspergen, G. R., Krauss, K. W., Reef, R., et al. (2015). The vulnerability of Indo-Pacific mangrove forests to sea-level rise. *Nature*, *526*(7574), 559–563. https://doi.org/10.1038/nature15538

Lovelock, C. E., & Reef, R. (2020). Variable impacts of climate change on blue carbon. *One Earth*, *3*(Number 2), 195–211. https://doi.org/10.1016/j.oneear.2020.07.010

Lovelock, C. E., Sorrell, B. K., Hancock, N., Hua, Q., & Swales, A. (2010). Mangrove forest and soil development on a rapidly accreting shore in New Zealand. *Ecosystems*, *13*(3), 437–451. https://doi.org/10.1007/s10021-010-9329-2

Lugo, A. E., & Snedaker, S. C. (1974). The ecology of mangroves. *Annual Review of Ecology and Systematics*, *5*(1), 39–64. https://doi.org/10.1146/annurev.es.05.110174.000351

Mack, S. K., Lane, R. R., Deng, J., Morris, J. T., & Bauer, J. J. (2023). Wetland carbon models: Applications for wetland carbon commercialization. *Ecological Modelling*, *476*, 110228. https://doi.org/10.1016/j.ecolmodel.2022.110228

Macreadie, P. I., Anton, A., Raven, J. A., Beaumont, N., Connolly, R. M., Friess, D. A., et al. (2019). The future of Blue Carbon science. In *Nature communications* (Vol. 10, (Iss. 1)). 3998, https://doi.org/10.1038/s41467-019-11693-w

Marciano, R., Wang, Z. B., Hibma, A., De Vriend, H. J., & Defina, A. (2005). Modeling of channel patterns in short tidal basins. *Journal of Geophysical Research*, *110*(1), F01001. https://doi.org/10.1029/2003JF000092

McKee, K., Rogers, K., & Saintilan, N. (2012). Response of salt marsh and mangrove wetlands to changes in atmospheric CO2, climate, and sea level. In *Global change and the function and distribution of wetlands*. https://doi.org/10.1007/978-94-007-4494-3_2

McKee, K. L. (2011). Biophysical controls on accretion and elevation change in Caribbean mangrove ecosystems. *Estuarine, Coastal and Shelf Science*, *91*(4), 475–483. https://doi.org/10.1016/j.ecss.2010.05.001

Mckee, K. L., Cahoon, D. R., & Feller, I. C. (2007). Caribbean mangroves adjust to rising sea level through biotic controls on change in soil elevation. *Global Ecology and Biogeography*, *16*(5), 545–556. https://doi.org/10.1111/j.1466-8238.2007.00317.x

McKee, K. L., Krauss, K. W., & Cahoon, D. R. (2020). Does geomorphology determine vulnerability of mangrove coasts to sea-level rise? In *Dynamic sedimentary environments of mangrove coasts*. https://doi.org/10.1016/B978-0-12-816437-2.00005-7

McLeod, E., Chmura, G. L., Bouillon, S., Salm, R., Björk, M., Duarte, C. M., et al. (2011). A blueprint for blue carbon: Toward an improved understanding of the role of vegetated coastal habitats in sequestering CO2. *Frontiers in Ecology and the Environment*, *9*(10), 552–560. https://doi.org/10.1890/110004

Meng, Y., Bai, J., Gou, R., Cui, X., Feng, J., Dai, Z., et al. (2021). Relationships between above- and below-ground carbon stocks in mangrove forests facilitate better estimation of total mangrove blue carbon. *Carbon Balance and Management*, *16*(1), 8. https://doi.org/10.1186/s13021-021-00172-9

Mizanur Rahman, M., Nabiul Islam Khan, M., Fazlul Hoque, A. K., & Ahmed, I. (2015). Carbon stock in the Sundarbans mangrove forest: Spatial variations in vegetation types and salinity zones. *Wetlands Ecology and Management*, *23*(2), 269–283. https://doi.org/10.1007/s11273-014-9379-x

Morris, J. T., Langley, J. A., Vervaeke, W. C., Dix, N., Feller, I. C., Marcum, P., & Chapman, S. K. (2023). Mangrove trees outperform saltmarsh grasses in building elevation but collapse rapidly under high rates of sea-level rise. *Earth's Future*, *11*(4), e2022EF003202. https://doi.org/10.1029/2022EF003202

Murray, A. B. (2007). Reducing model complexity for explanation and prediction. *Geomorphology*, *90*(3–4), 178–191. https://doi.org/10.1016/j.geomorph.2006.10.020

Murray, A. B. (2013). Which models are good (Enough), and when? In *Treatise on geomorphology* (Vol. 1–14, pp. 1–14). https://doi.org/10.1016/B978-0-12-374739-6.00027-0

Nardin, W., Vona, I., & Fagherazzi, S. (2021). Sediment deposition affects mangrove forests in the Mekong delta, Vietnam. *Continental Shelf Research*, *213*, 104319. https://doi.org/10.1016/j.csr.2020.104319

Osland, M. J., Chivoiu, B., Grace, J. B., Enwright, N. M., Guntenspergen, G. R., Buffington, K. J., et al. (2024). Rising seas could cross thresholds for initiating coastal wetland drowning within decades across much of the United States. *Communications Earth & Environment*, *5*(1), 372. https://doi.org/10.1038/s43247-024-01537-x

Owers, C. J., Rogers, K., Mazumder, D., & Woodroffe, C. D. (2020). Temperate coastal wetland near-surface carbon storage: Spatial patterns and variability. *Estuarine, Coastal and Shelf Science*, *235*, 106584. https://doi.org/10.1016/j.ecss.2020.106584

Partheniades, E. (1965). Erosion and deposition of cohesive soils. *Journal of the Hydraulics Division*, *91*(1), 105–139. https://doi.org/10.1061/jyceaj.0001165

Parton, W. J., Schimel, D. S., Cole, C. V., & Ojima, D. S. (1987). Analysis of factors controlling soil organic matter levels in Great Plains grasslands. *Soil Science Society of America Journal*, *51*(5), 1173–1179. https://doi.org/10.2136/sssaj1987.03615995005100050015x

Peters, R., Walther, M., Lovelock, C., Jiang, J., & Berger, U. (2020). The interplay between vegetation and water in mangroves: New perspectives for mangrove stand modelling and ecological research. In *Wetlands ecology and management* (Vol. 28, (Iss. 4), pp. 697–712). https://doi.org/10.1007/s11273-020-09733-0

Pool, D. J., Lugo, A. E., & Snedaker, S. C. (1975). Litter production in mangrove forests of southern Florida and Puerto Rico. *Proceedings of the International Symposium on Biology and Management of Mangroves*, *1*, 213–237.

Porté, A., & Bartelink, H. H. (2002). Modelling mixed forest growth: A review of models for forest management. *Ecological Modelling*, *150*(1–2), 141–188. https://doi.org/10.1016/S0304-3800(01)00476-8

Pörtner, H.-O., Roberts, D. C., Masson-Delmotte, V., Zhai, P., Tignor, M., Poloczanska, E., et al. (2019). The Ocean and cryosphere in a changing climate: A special report of the intergovernmental panel on climate change. In The Ocean and Cryosphere in a changing climate (October). Retrieved from https://www.ipcc.ch/srocc/chapter/summary-for-policymakers/

Puppin, A., Tognin, D., Ghinassi, M., Franceschinis, E., Realdon, N., Marani, M., & D'Alpaos, A. (2023). *Spatial and vertical patterns of Soil Organic Matter and Carbon content in the salt marshes of the Venice Lagoon (Italy)*. EGUsphere.

Reef, R., Feller, I. C., & Lovelock, C. E. (2010). Nutrition of mangroves. *Tree Physiology*, *30*(9), 1148–1160. https://doi.org/10.1093/treephys/tpq048

Restrepo, J. C., Schrottke, K., Traini, C., Ortíz, J. C., Orejarena, A., Otero, L., et al. (2016). Sediment transport and geomorphological change in a high-discharge tropical delta (Magdalena River, Colombia): Insights from a period of intense change and human intervention (1990-2010). *Journal of Coastal Research*, *32*(3), 575–589. https://doi.org/10.2112/JCOASTRES-D-14-00263.1

Robertson, A. I., & Daniel, P. A. (1989). Decomposition and the annual flux of detritus from fallen timber in tropical mangrove forests. *Limnology and Oceanography*, *34*(3), 640–646. https://doi.org/10.4319/lo.1989.34.3.0640

Rogers, K. (2021). Accommodation space as a framework for assessing the response of mangroves to relative sea-level rise. *Singapore Journal of Tropical Geography*, *42*(2), 163–183. https://doi.org/10.1111/sjtg.12357

Rogers, K., Kelleway, J. J., Saintilan, N., Megonigal, J. P., Adams, J. B., Holmquist, J. R., et al. (2019). Wetland carbon storage controlled by millennial-scale variation in relative sea-level rise. *Nature*, *567*(7746), 91–95. https://doi.org/10.1038/s41586-019-0951-7

Roner, M., D'Alpaos, A., Ghinassi, M., Marani, M., Silvestri, S., Franceschinis, E., & Realdon, N. (2016). Spatial variation of salt-marsh organic and inorganic deposition and organic carbon accumulation: Inferences from the Venice lagoon, Italy. *Advances in Water Resources*, *93*, 276–287. https://doi.org/10.1016/j.advwatres.2015.11.011

Rosentreter, J. A., Maher, D. T., Erler, D. V., Murray, R., & Eyre, B. D. (2018). Seasonal and temporal CO2 dynamics in three tropical mangrove creeks – A revision of global mangrove CO2 emissions. *Geochimica et Cosmochimica Acta*, *222*, 729–745. https://doi.org/10.1016/j.gca.2017.11.026

Rovai, A. S., Twilley, R. R., Castañeda-Moya, E., Riul, P., Cifuentes-Jara, M., Manrow-Villalobos, M., et al. (2018). Global controls on carbon storage in mangrove soils. *Nature Climate Change*, *8*(6), 534–538. https://doi.org/10.1038/s41558-018-0162-5

Saintilan, N. (1997). Above- and below-ground biomass of mangroves in a sub-tropical estuary. *Marine and Freshwater Research*, *48*(7), 601–604. https://doi.org/10.1071/MF97009

Saintilan, N., Khan, N. S., Ashe, E., Kelleway, J. J., Rogers, K., Woodroffe, C. D., & Horton, B. P. (2020). Thresholds of mangrove survival under rapid sea level rise. *Science*, *368*(6495), 1118–1121. https://doi.org/10.1126/science.aba2656

Saintilan, N., Rogers, K., Mazumder, D., & Woodroffe, C. (2013). Allochthonous and autochthonous contributions to carbon accumulation and carbon store in southeastern Australian coastal wetlands. *Estuarine, Coastal and Shelf Science*, *128*, 84–92. https://doi.org/10.1016/j.ecss.2013.05.010

Sanderman, J., Hengl, T., Fiske, G., Solvik, K., Adame, M. F., Benson, L., et al. (2018). A global map of mangrove forest soil carbon at 30 m spatial resolution. *Environmental Research Letters*, *13*(5), 055002. https://doi.org/10.1088/1748-9326/aabe1c

Sandi, S. G., Rodriguez, J. F., Saco, P. M., Saintilan, N., & Riccardi, G. (2021). Accelerated sea-level rise limits vegetation capacity to sequester soil carbon in coastal wetlands: A Study case in Southeastern Australia. *Earth's Future*, *9*(9), e2020EF001901. https://doi.org/10.1029/2020EF001901

Sanford, L. P. (2008). Modeling a dynamically varying mixed sediment bed with erosion, deposition, bioturbation, consolidation, and armoring. *Computers and Geosciences*, *34*(10), 1263–1283. https://doi.org/10.1016/j.cageo.2008.02.011

Sasmito, S. D., Murdiyarso, D., Friess, D. A., & Kurnianto, S. (2016). Can mangroves keep pace with contemporary sea level rise? A global data review. *Wetlands Ecology and Management*, *24*(2), 263–278. https://doi.org/10.1007/s11273-015-9466-7

Schuerch, M., Spencer, T., Temmerman, S., Kirwan, M. L., Wolff, C., Lincke, D., et al. (2018). Future response of global coastal wetlands to sea-level rise. *Nature*, *561*(7722), 231–234. https://doi.org/10.1038/s41586-018-0476-5

Schwarz, C., van Rees, F., Xie, D., Kleinhans, M. G., & van Maanen, B. (2022). Salt marshes create more extensive channel networks than mangroves. *Nature Communications*, *13*(1), 2017. https://doi.org/10.1038/s41467-022-29654-1

Sharma, R., Mishra, D. R., Levi, M. R., & Sutter, L. A. (2022). Remote sensing of surface and subsurface soil organic carbon in tidal wetlands: A review and ideas for future research. *Remote Sensing*, *14*(12), 2940. https://doi.org/10.3390/rs14122940

Suello, R. H., Temmerman, D., Bouillon, S., Khalifeh, Z., van Puijenbroek, M., Elschot, K., et al. (2025). Increased sea level rise accelerates carbon sequestration in a macro-tidal salt marsh. *Science of The Total Environment*, *958*, 178075. https://doi.org/10.1016/j.scitotenv.2024.178075

Syvitski, J. P. M., Kettner, A. J., Overeem, I., Hutton, E. W. H., Hannon, M. T., Brakenridge, G. R., et al. (2009). Sinking deltas due to human activities. *Nature Geoscience*, *2*(10), 681–686. https://doi.org/10.1038/ngeo629

Twilley, R. R., Lugo, A. E., & Patterson-Zucca, C. (1986). Litter production and turnover in basin mangrove forests in southwest Florida. *Ecology*, *67*(3), 670–683. https://doi.org/10.2307/1937691

Twilley, R. R., Pozo, M., Garcia, V. H., Rivera-Monroy, V. H., Zambrano, R., & Bodero, A. (1997). Litter dynamics in riverine mangrove forests in the Guayas river estuary, Ecuador. *Oecologia*, *111*(1), 109–122. https://doi.org/10.1007/s004420050214

Twilley, R. R., Rovai, A. S., & Riul, P. (2018). Coastal morphology explains global blue carbon distributions. *Frontiers in Ecology and the Environment*, *16*(9), 503–508. https://doi.org/10.1002/fee.1937

van Hespen, R., Hu, Z., Borsje, B., De Dominicis, M., Friess, D. A., Jevrejeva, S., et al. (2023). Mangrove forests as a nature-based solution for coastal flood protection: Biophysical and ecological considerations. *Water Science and Engineering*, *16*(1), 1–13. https://doi.org/10.1016/j.wse.2022.10.004

Van Maanen, B., Coco, G., & Bryan, K. R. (2013). Modelling the effects of tidal range and initial bathymetry on the morphological evolution of tidal embayments. *Geomorphology*, *191*, 23–34. https://doi.org/10.1016/j.geomorph.2013.02.023

Van Maanen, B., Coco, G., & Bryan, K. R. (2015). On the ecogeomorphological feedbacks that control tidal channel network evolution in a sandy mangrove setting. *Proceedings of the Royal Society A: Mathematical, Physical and Engineering Sciences*, *471*(2180), 20150115. https://doi.org/10.1098/rspa.2015.0115

van Oorschot, M., Kleinhans, M., Geerling, G., & Middelkoop, H. (2016). Distinct patterns of interaction between vegetation and morphodynamics. *Earth Surface Processes and Landforms*, *41*(6), 791–808. https://doi.org/10.1002/esp.3864

Vo, Q. T., Kuenzer, C., Vo, Q. M., Moder, F., & Oppelt, N. (2012). Review of valuation methods for mangrove ecosystem services. *Ecological Indicators*, *23*, 431–446. https://doi.org/10.1016/j.ecolind.2012.04.022

Volta, C., Ho, D. T., Maher, D. T., Wanninkhof, R., Del Castillo, C., Del Castillo, C., & Dulai, H. (2020). Seasonal variations in dissolved carbon inventory and fluxes in a mangrove-dominated Estuary. *Global Biogeochemical Cycles*, *34*(12), e2019GB006515. https://doi.org/10.1029/2019GB006515

Wang, F., Lu, X., Sanders, C. J., & Tang, J. (2019). Tidal wetland resilience to sea level rise increases their carbon sequestration capacity in United States. *Nature Communications*, *10*(1), 5434. https://doi.org/10.1038/s41467-019-13294-z

Wang, F., Sanders, C. J., Santos, I. R., Tang, J., Schuerch, M., Kirwan, M. L., et al. (2021). Global blue carbon accumulation in tidal wetlands increases with climate change. *National Science Review*, *8*(9), nwaa296. https://doi.org/10.1093/nsr/nwaa296

Wang, G., Guan, D., Peart, M. R., Chen, Y., & Peng, Y. (2013). Ecosystem carbon stocks of mangrove forest in Yingluo Bay, Guangdong Province of South China. *Forest Ecology and Management*, *310*, 539–546. https://doi.org/10.1016/j.foreco.2013.08.045

Wang, J., Yu, G., Ding, H., Liu, T., Chen, X., & Zhang, X. (2025). Current status of coastal blue carbon assessment: Theory, methods, and carbon sequestration pathways. *Science China Earth Sciences*, *68*(5), 1403–1418. https://doi.org/10.1007/s11430-024-1542-8

Wei, Y., van Maanen, B., Xie, D., Jiang, Q., Zhou, Z., & Schwarz, C. (2024). Mangrove-Saltmarsh ecotones: Are species shifts determining eco-morphodynamic landform configurations? *Earth's Future*, *12*(10), e2024EF004990. https://doi.org/10.1029/2024EF004990

Wicaksono, P., Danoedoro, P., Hartono, & Nehren, U. (2016). Mangrove biomass carbon stock mapping of the Karimunjawa Islands using multispectral remote sensing. *International Journal of Remote Sensing*, *37*(1), 26–52. https://doi.org/10.1080/01431161.2015.1117679

Wolf, A. A., Drake, B. G., Erickson, J. E., & Megonigal, J. P. (2007). An oxygen-mediated positive feedback between elevated carbon dioxide and soil organic matter decomposition in a simulated anaerobic wetland. *Global Change Biology*, *13*(9), 2036–2044. https://doi.org/10.1111/j.1365-2486.2007.01407.x

Woodroffe, C. D., Rogers, K., McKee, K. L., Lovelock, C. E., Mendelssohn, I. A., & Saintilan, N. (2016). Mangrove sedimentation and response to relative sea-level rise. *Annual Review of Marine Science*, *8*(1), 243–266. https://doi.org/10.1146/annurev-marine-122414-034025

Worthington, T. A., zu Ermgassen, P. S. E., Friess, D. A., Krauss, K. W., Lovelock, C. E., Thorley, J., et al. (2020). A global biophysical typology of mangroves and its relevance for ecosystem structure and deforestation. *Scientific Reports*, *10*(1), 14652. https://doi.org/10.1038/s41598-020-71194-5

Xie, D., Schwarz, C., Brückner, M. Z. M., Kleinhans, M. G., Urrego, D. H., Zhou, Z., & van Maanen, B. (2020). Mangrove diversity loss under sea-level rise triggered by bio-morphodynamic feedbacks and anthropogenic pressures. *Environmental Research Letters*, *15*(11), 114033. https://doi.org/10.1088/1748-9326/abc122

Xie, D., Schwarz, C., Kleinhans, M. G., Bryan, K. R., Coco, G., Hunt, S., & van Maanen, B. (2023). Mangrove removal exacerbates estuarine infilling through landscape-scale bio-morphodynamic feedbacks. *Nature Communications*, *14*(1), 7310. https://doi.org/10.1038/s41467-023-42733-1

Xie, D., Schwarz, C., Kleinhans, M. G., Zhou, Z., & van Maanen, B. (2022). Implications of coastal conditions and sea-level rise on mangrove vulnerability: A bio-morphodynamic modeling Study. *Journal of Geophysical Research: Earth Surface*, *127*(3), e2021JF006301. https://doi.org/10.1029/2021JF006301

Zhang, J., Gan, S., Yang, P., Zhou, J., Huang, X., Chen, H., et al. (2024). A global assessment of mangrove soil organic carbon sources and implications for blue carbon credit. *Nature Communications*, *15*(1), 8994. https://doi.org/10.1038/s41467-024-53413-z

Zhou, Z., Coco, G., Jiménez, M., Olabarrieta, M., Van Der Wegen, M., & Townend, I. (2014). Morphodynamics of river-influenced back-barrier tidal basins: The role of landscape and hydrodynamic settings. *Water Resources Research*, *50*(12), 9514–9535. https://doi.org/10.1002/2014WR015891

Zhou, Z., Coco, G., van der Wegen, M., Gong, Z., Zhang, C., & Townend, I. (2015). Modeling sorting dynamics of cohesive and non-cohesive sediments on intertidal flats under the effect of tides and wind waves. *Continental Shelf Research*, *104*, 76–91. https://doi.org/10.1016/j.csr.2015.05.010

Zhou, Z., Ye, Q., & Coco, G. (2016). A one-dimensional biomorphodynamic model of tidal flats: Sediment sorting, marsh distribution, and carbon accumulation under sea level rise. *Advances in Water Resources*, *93*, 288–302. https://doi.org/10.1016/j.advwatres.2015.10.011

References From the Supporting Information

Castaneda-Moya, E., Twilley, R. R., Rivera-Monroy, V. H., Marx, B. D., CoronadoMolina, C., & Ewe, S. M. L. (2011). Patterns of root dynamics in mangrove forests along environmental gradients in the Florida coastal everglades, USA. *Ecosystems*, *14*(7). https://doi.org/10.1007/s10021-011-9473-3

Iwantoro, A. P., Van Der Vegt, M., & Kleinhans, M. G. (2020). Morphological evolution of bifurcations in tide-influenced deltas. *Earth Surface Dynamics*, *8*(2), 413–429. https://doi.org/10.5194/esurf-8-413-2020